

# On the Identification of Diagnostic Expectations: Econometric Insights from DSGE Models

Jinting Guo\*

September 11, 2025

## Abstract

This paper provides the first econometric evidence for diagnostic expectations (DE) in DSGE models. Using the identification framework of [Qu and Tkachenko \(2017\)](#), I show that DE generate dynamics unattainable under rational expectations (RE), with no RE parameterization capable of matching the volatility and persistence patterns implied by DE. Consequently, DE are not observationally equivalent to RE and constitute an endogenous source of macroeconomic fluctuations, distinct from both structural frictions and exogenous shocks. From an econometric perspective, DE preserve overall model identification but weaken the identification of shock variances. To ensure robust conclusions across estimation methods and equilibrium conditions, I extend Bayesian estimation with Sequential Monte Carlo sampling to the indeterminacy domain. These findings advance the econometric study of expectations and highlight the macroeconomic relevance of diagnostic beliefs.

*JEL classification:* C11; C13; C54; C63; E71

*Keywords:* Diagnostic expectations; DSGE; Identification;

---

\*PhD candidate at Goethe University Frankfurt. E-mail: [jinting.guo@stud.uni-frankfurt.de](mailto:jinting.guo@stud.uni-frankfurt.de). I am especially grateful to Denis Tkachenko for being supportive throughout this project. I am also grateful to Michael Binder (1st supervisor), Alexander Meyer-Gohde (2nd supervisor), Uwe Hassler, Ina Krapp, Yulei Luo, Alberto Martin, Hashem Pesaran, Davide Raggi, Ludwig Straub, Penghui Yin, Donghoon Yoo and the member of Monetary Policy and Analysis Division at the Bundesbank for helpful discussion and comments. I further benefited from feedback provided by participants at the 15th RCEA Bayesian Econometrics Workshop, the 13th Annual Conference of the International Association for Applied Econometrics, and the 2nd Frankfurt Summer School. Any remaining errors are my own.

# 1 Introduction

Expectations are central to modern macroeconomic theory, shaping household consumption and saving decisions as well as firms' pricing and investment strategies. For decades, the prevailing assumption has been that these expectations are formed rationally. More recently, however, diagnostic expectations (DE) have emerged as an influential alternative. This framework offers new insights into the overreaction, volatility, and cyclical patterns that characterize both financial markets and macroeconomic dynamics. Building on [Kahneman and Tversky \(1972\)](#)'s representativeness heuristic, [Bordalo et al. \(2018\)](#) introduced DE to capture the psychological tendency to overestimate future outcomes that appear more likely in light of incoming information.

While theoretical research has highlighted the potential of DE to explain macroeconomic phenomena, key empirical questions remain: Can DE be reliably identified in standard macroeconomic models, and do they generate dynamics that are truly distinct from rational expectations (RE)? Moreover, is the overreaction produced by DE empirically distinguishable from other amplification channels? This paper provides the first comprehensive econometric analysis to address these questions within both small- and medium-scale log-linearized DSGE models. Such analysis is essential for establishing DE as a viable alternative to RE in macroeconomic modeling.

I begin with a small-scale DSGE framework and show that the diagnostic parameter can be identified globally using the frequency domain methodology of [Qu and Tkachenko \(2017\)](#). This approach introduces a frequency domain expression for the Kullback–Leibler (KL) distance between two DSGE models, which measures the difference between their implied spectra (the frequency domain representation of the autocovariance functions). If no two parameter sets generate identical spectrum, that is, if the KL distance is strictly positive, the model is globally identified. Applying this criterion, I find that incorporating DE does not compromise overall model identification but systematically weakens the identification of shock variances. By contrast, key structural parameters remain well identified. This pattern is consistent with the theoretical structure of DE: the diagnostic parameter alters only the shock impact coefficients while leaving autoregressive dynamics unchanged, thereby reducing the sensitivity of the model implied spectrum to changes in shock variances.

I then examine whether RE can replicate DE dynamics within this small-scale framework. To do so, I allow all structural parameters in the RE model to vary freely in order to match the DE-implied spectrum. Despite this flexibility, no RE parameterization can reproduce a spectrum sufficiently close to that of the DE model, with positive KL distances remaining both theoretically and statistically significant. This exercise yields a set of RE parameters that generate dynamics closest to those under DE. The associated impulse responses reveal the underlying mechanism: DE operates as a behavioral extrapolation channel, generating endogenous, expectation-driven amplification rather than relying solely on exogenous shock variance or persistence under RE.

Next, I extend the analysis to a medium-scale DSGE model with investment adjustment costs, variable capital utilization, habit persistence, and wage stickiness. This richer setting confirms the robustness of the findings from small-scale model and provides an opportunity to study alternative overreaction channels. While these structural frictions can partially substitute for DE by shifting dynamics into other mechanisms, none can fully replicate the benchmark DE dynamics. This highlights expectation formation as a distinct dimension of macroeconomic modeling, complementary to rather than substitutable by structural frictions and exogenous shocks. Moreover, by examining identification strength at both the full spectrum and business cycle frequencies, I show that the results are not driven by potentially misspecified low frequency components, ensuring robustness across frequency domains.

Finally, I contribute methodologically by extending Bayesian estimation with Sequential Monte Carlo (SMC) sampling to the indeterminacy domain. This extension enables a systematic robustness check of identification across estimation methods and equilibrium conditions.

**Related literature.** This paper relates to two strands of literature: the literature on DE and the broader research on the identification of structural parameters in macroeconomic models. The first strand relates to the growing body of research on DE. [Bordalo et al. \(2018\)](#) (BGS) introduce DE to explain several features of credit cycles, demonstrating how agents' psychological tendency to overweight representative future outcomes amplifies economic fluctuations. [Bordalo et al. \(2020\)](#) explore DE with dispersed information, finding that agents overreact to private signals while underreacting to consensus forecasts. [Bordalo et al. \(2021\)](#) incorporate price learning and speculative behavior, accounting for the underreaction-

overshooting-crash pattern in asset price bubbles. [Guo et al. \(2023\)](#) examine DE under incomplete information and document excess consumption sensitivity consistent with survey evidence. More recently, [Bianchi et al. \(2024a\)](#) show that a DE-based RBC model better replicates boom-bust cycles compared to its rational expectations counterpart. [Na and Yoo \(2025\)](#) apply this approach to study countercyclical external balances in emerging markets. [L’Huillier et al. \(2024\)](#) incorporate DE into a New Keynesian framework, providing a foundation for my identification analysis. While recent contributions propose smooth DE that distortion vary with uncertainty ([Bianchi et al., 2024b](#)), this paper employs the standard BGS framework, which remains the theoretical foundation for most research in this area.

Another strand of research focuses on the identification of DSGE models. [Canova and Sala \(2009\)](#) highlight that observational equivalence, partial, and weak identification are widespread in DSGE models, often arising from an ill-behaved mapping between structural parameters and solution coefficients. [Iskrev \(2010\)](#) later developed a rank condition providing a sufficient condition for local identification, while [Komunjer and Ng \(2011\)](#) proposed a Jacobian rank condition offering necessary and sufficient criteria. [Qu and Tkachenko \(2012\)](#) extended this literature by formulating a frequency-domain rank condition for local identification. Additionally, [Koop et al. \(2013\)](#) introduced prior-posterior comparison and posterior learning rate indicators as tools for assessing local identification. Research on global identification emerged later. [Qu and Tkachenko \(2017\)](#) addressed this issue in the frequency domain by examining the KL divergence between two DSGE models, providing a framework to assess identification beyond local conditions. More recently, [Kocięcki and Kolasa \(2023\)](#) proposed an analytical solution for global identification using Gröbner basis methods, offering a systematic approach to solving polynomial restrictions in DSGE models.

This paper follows the approach of [Qu and Tkachenko \(2017\)](#). Their methodology is well suited for analyzing identification across different model structures, such as RE versus DE, and for comparing DE with other overreaction channels. This is crucial for establishing whether DE generates dynamics that cannot be replicated under RE and whether it is empirically distinguishable from alternative amplification mechanisms. The method has further advantages. It allows identification analysis at specific frequency ranges, enabling a focus on the business cycle frequencies that is most relevant to DSGE models. It also provides a structured framework to quantify identification strength, offering insights into

which parameters can be estimated most reliably.

The remainder of the paper is organized as follows. Section 2 reviews the theoretical foundations of diagnostic expectations and their implementation in DSGE models. Section 3 presents our identification analysis for a small-scale DSGE model, while Section 4 extends the analysis to a medium-scale model. Section 5 concludes the paper.

## 2 Diagnostic Expectation

In this section, I will briefly introduce DE and summarize the practical calculation properties for solving the DSGE system. [Bordalo et al. \(2018\)](#) first formalized the DE for an exogenous economic state variable following AR(1) process. Assume the economic state at  $t$  is  $\omega_t$  following a AR(1) process  $\omega_t = \rho\omega_{t-1} + \varepsilon_t$ , where  $\varepsilon_t \sim N(0, \sigma_\varepsilon^2)$  and  $\rho \in (0, 1]$  is the persistent parameter. The more representative future state is the one more likely to occur under the realized state  $G \equiv \{\omega_t = \hat{\omega}_t\}$  than based on the referenced past  $-G \equiv \{\omega_t = \rho\hat{\omega}_{t-1}\}$ . Hence, the representativeness can be written as a division of the two conditional probability distributions  $\frac{f(\hat{\omega}_{t+1}|G_t)}{f(\hat{\omega}_{t+1}|-G_t)}$ . When DE agents make their expectations, they have the true conditional expectation in mind but inflate the probability of the representative future state and deflate the less representative one. Therefore, the diagnostic distribution (or the distorted pdf) of  $\omega_{t+1}$  is defined as true distribution times the representative-distortion term

$$f_t^\theta(\hat{\omega}_{t+1}) = f(\hat{\omega}_{t+1}|G_t) \left[ \frac{f(\hat{\omega}_{t+1}|G_t)}{f(\hat{\omega}_{t+1}|-G_t)} \right]^\theta \cdot C, \quad (1)$$

where  $C$  is a constant ensuring  $f_t^\theta$  integrate to 1 and  $\theta$  measures the distortion severity. If  $\theta = 0$ , then representative distortion shuts down, we are going back to the RE case. If  $\theta > 0$ , the larger the  $\theta$ , the larger overweighting of the representative state. Denote the diagnostic expectation operator at time  $t$  by  $E_t^\theta$ , it can be formally defined as

$$E_t^\theta[\omega_{t+1}] = \int_{-\infty}^{\infty} \omega f_t^\theta(\omega) d\omega. \quad (2)$$

Since  $\omega_t$  follows a AR(1) process with  $N(0, \sigma_\varepsilon^2)$  shocks, it is very crucial to point out that the diagnostic distribution is also normal. Thus DE has a RE representation<sup>1</sup>

$$E_t^\theta(\omega_{t+1}) = E_t\omega_{t+1} + \theta[E_t\omega_{t+1} - E_{t-1}\omega_{t+1}]. \quad (3)$$

The RE representation also holds for the multivariate case (L'Huillier et al., 2024).

Although the original analysis of DE lies on autoregressive exogenous variables (Bordalo et al., 2018), studying the DE for endogenous variables is crucial for solving economic models like the DSGE model with DE agents. L'Huillier et al. (2024) propose a solution method that solves a stochastic difference equation system combining both exogenous and endogenous variables. Suppose the SDE is

$$E_t^\theta[\mathbf{F}\mathbf{y}_{t+1} + \mathbf{G}_1\mathbf{y}_t + \mathbf{M}\mathbf{x}_{t+1} + \mathbf{N}_1\mathbf{x}_t] + \mathbf{G}_2\mathbf{y}_t + \mathbf{H}\mathbf{y}_{t-1} + \mathbf{N}_2\mathbf{x}_t = 0 \quad (4)$$

where exogenous variables are stacked in a  $(n \times 1)$  vector  $\mathbf{x}_t$  following a AR(1) stochastic process, i.e.,  $\mathbf{x}_t = \mathbf{A}\mathbf{x}_{t-1} + \boldsymbol{\nu}_t$  and  $\mathbf{A}$  is a diagonal matrix of persistence parameters,  $\boldsymbol{\nu}_t \sim N(0, \Sigma_\nu)$ ;  $\mathbf{y}_t$  is a  $(m \times 1)$  vector of endogenous variables;  $\mathbf{F}_{m \times m}$ ,  $(\mathbf{G}_1)_{m \times m}$ ,  $(\mathbf{G}_2)_{m \times m}$ ,  $\mathbf{H}_{m \times m}$ ,  $(\mathbf{N}_1)_{m \times n}$  and  $(\mathbf{N}_2)_{m \times n}$  are matrices of parameters.

To write the RE representation for SDE combined with exogenous and endogenous variables, L'Huillier et al. (2024) guess a solution according to the extrapolative nature of DE, i.e.,  $\mathbf{y}_t = \mathbf{P}\mathbf{y}_{t-1} + \mathbf{Q}\mathbf{x}_t + \mathbf{R}\boldsymbol{\nu}_t$ . After verification, they show it indeed constitutes a solution for SDE.<sup>2</sup> Note that the solution has a very good property in that it follows a multivariate normal distribution. Hence using the same technology as exogenous normal distributed variables, the DE-SDE has the following RE representation

$$\begin{aligned} & \mathbf{F}E_t[\mathbf{y}_{t+1}] + \mathbf{G}\mathbf{y}_t + \mathbf{H}\mathbf{y}_{t-1} + \mathbf{M}E_t[\mathbf{x}_{t+1}] + \mathbf{N}\mathbf{x}_t + \mathbf{F}\theta(E_t[\mathbf{y}_{t+1}] - E_{t-1}[\mathbf{y}_{t+1}]) \\ & + \mathbf{M}\theta(E_t[\mathbf{x}_{t+1}] - E_{t-1}[\mathbf{x}_{t+1}]) + \mathbf{G}_1\theta(\mathbf{y}_t - E_{t-1}[\mathbf{y}_t]) + \mathbf{N}_1\theta(\mathbf{x}_t - E_{t-1}[\mathbf{x}_t]) = 0 \end{aligned} \quad (5)$$

where  $\mathbf{G} = \mathbf{G}_1 + \mathbf{G}_2$ ,  $\mathbf{N} = \mathbf{N}_1 + \mathbf{N}_2$ .

---

<sup>1</sup>Proof see the Internet Appendix of Bordalo et al. (2018). It is also shown in the appendix that the property can easily expand to the case where  $\omega_t$  follows a AR(N) process.

<sup>2</sup>Details see the appendix of L'Huillier et al. (2024).

### 3 Identification analysis for a small-scale DSGE

In this section, I examine both local and global identification of the diagnostic parameter  $\theta$  in the small-scale DSGE model of [L’Huillier et al. \(2024\)](#). The model is specified as follows:

$$\hat{y}_t = E_t^\theta[\hat{y}_{t+1}] - (\hat{i}_t - E_t^\theta[\hat{\pi}_{t+1}]) + \theta(\hat{\pi}_t - E_{t-1}[\hat{\pi}_t]) + \hat{g}_t - E_t^\theta[\hat{g}_{t+1}] \quad (6)$$

$$\hat{\pi}_t = \beta E_t^\theta[\hat{\pi}_{t+1}] + \kappa(\hat{y}_t - \hat{a}_t) - \frac{\kappa}{1+\nu}\hat{g}_t \quad (7)$$

$$\hat{i}_t = \phi_\pi \hat{\pi}_t + \phi_y(\hat{y}_t - \hat{a}_t) + \varepsilon_{m,t}, \quad (8)$$

with shock processes:

$$\hat{a}_t = \rho_a \hat{a}_{t-1} + \varepsilon_{a,t} \quad (9)$$

$$\hat{g}_t = \rho_g \hat{g}_{t-1} + \varepsilon_{g,t} \quad (10)$$

Note that a monetary policy shock,  $\varepsilon_{m,t}$ , has been added to square the system.

#### 3.1 The spectrum of a DSGE model

To compute the spectrum of a DSGE model, it is necessary first to derive its solution. As detailed in Section 2, the DE-NK model can be reformulated into an equivalent RE representation, thereby permitting the use of conventional solution techniques. To maintain clarity, all detailed matrices and intermediate steps are omitted from the main text and provided in the Online Appendix. For the model presented above, I express it in RE form as follows:

$$\begin{aligned} & (1 + \theta)E_t[\hat{y}_{t+1}] + (1 + \theta)E_t[\hat{\pi}_{t+1}] - \hat{y}_t - \hat{i}_t + \hat{g}_t + \theta\hat{\pi}_t - (1 + \theta)E_t[\hat{g}_{t+1}] \\ & = \theta E_{t-1}[\hat{y}_{t+1}] + \theta E_{t-1}[\hat{\pi}_{t+1}] + \theta E_{t-1}[\hat{\pi}_t] - \theta E_{t-1}[\hat{g}_{t+1}], \\ & \hat{\pi}_t = \beta(1 + \theta)E_t[\hat{\pi}_{t+1}] - \beta\theta E_{t-1}[\hat{\pi}_{t+1}] + \kappa(\hat{y}_t - \hat{a}_t) - \frac{\kappa}{1+\nu}\hat{g}_t, \\ & \hat{i}_t = \phi_\pi \hat{\pi}_t + \phi_y(\hat{y}_t - \hat{a}_t) + \varepsilon_{m,t}, \\ & \hat{a}_t = \rho_a \hat{a}_{t-1} + \varepsilon_{a,t}, \quad \hat{g}_t = \rho_g \hat{g}_{t-1} + \varepsilon_{g,t}. \end{aligned} \quad (11)$$

Following [Sims \(2002\)](#), I solve this DSGE system by employing Sims's canonical form:

$$\mathbf{\Gamma}_0 \mathbf{S}_t = \mathbf{\Gamma}_1 \mathbf{S}_{t-1} + \mathbf{C} + \mathbf{\Psi} \mathbf{z}_t + \mathbf{\Pi} \boldsymbol{\eta}_t, \quad (12)$$

where  $\mathbf{S}_t$  denotes the state vector,  $\mathbf{C}$  is a vector of constants,  $\mathbf{z}_t$  represents exogenous shocks, and  $\boldsymbol{\eta}_t$  corresponds to expectation errors satisfying  $E_t(\boldsymbol{\eta}_{t+1}) = 0$ . To accommodate the lagged expectation terms induced by DE, I expand the state vector to include four auxiliary variables:

$$\mathbf{S}_t = (\hat{y}_t, \hat{\pi}_t, P_t, X_t, Q_t, Y_t, \hat{i}_t, \hat{a}_t, \hat{g}_t)',$$

where  $P_t := E_t[\hat{y}_{t+1}]$ ,  $X_t := E_t[\hat{\pi}_{t+1}]$ ,  $Q_t := E_t[\hat{y}_{t+2}]$ , and  $Y_t := E_t[\hat{\pi}_{t+2}]$ . System (11) is augmented with four auxiliary equations:  $\hat{y}_t = P_{t-1} + \eta_t^y$ ,  $\hat{\pi}_t = X_{t-1} + \eta_t^\pi$ ,  $P_t = Q_{t-1} + \eta_t^P$ ,  $X_t = Y_{t-1} + \eta_t^X$ .

The full set of stable solutions to this system, as shown in [Lubik and Schorfheide \(2003\)](#), can be expressed as:

$$\mathbf{S}_t = \mathbf{\Theta}_1 \mathbf{S}_{t-1} + \mathbf{\Theta}_\varepsilon \boldsymbol{\varepsilon}_t + \mathbf{\Theta}_\epsilon \boldsymbol{\epsilon}_t, \quad (13)$$

where  $\mathbf{\Theta}_1$ ,  $\mathbf{\Theta}_\varepsilon$ , and  $\mathbf{\Theta}_\epsilon$  are functions of  $\mathbf{\Gamma}_0$ ,  $\mathbf{\Gamma}_1$ ,  $\mathbf{\Psi}$ , and  $\mathbf{\Pi}$ , all depending on the parameter vector  $\boldsymbol{\gamma}$ . Here,  $\boldsymbol{\epsilon}_t$  denotes sunspot shocks. As noted in [Lubik and Schorfheide \(2004\)](#), if the central bank's response to inflation is insufficiently aggressive (i.e.,  $\phi_\pi < 1$ ), sunspot shocks may influence macroeconomic dynamics, resulting in indeterminacy.

Allowing for correlation between sunspot shocks  $\boldsymbol{\epsilon}_t$  and structural shocks  $\boldsymbol{\varepsilon}_t$ , the following projection applies:

$$\boldsymbol{\epsilon}_t = \mathbf{M} \boldsymbol{\varepsilon}_t + \tilde{\boldsymbol{\epsilon}}_t, \quad (14)$$

where  $\mathbf{M} = E(\boldsymbol{\epsilon}_t \boldsymbol{\varepsilon}_t') [E(\boldsymbol{\varepsilon}_t \boldsymbol{\varepsilon}_t')]^{-1}$  represents the projection coefficients, and  $\tilde{\boldsymbol{\epsilon}}_t$  are the projection residuals.

To compute the spectral density, I map the observable vector  $\mathbf{Y}_t = (\hat{y}_t, \hat{\pi}_t, \hat{i}_t)'$  to the state vector  $\mathbf{S}_t$  using a selection matrix  $\mathbf{A}(L)$ . The state vector evolves according to equation (13) and depends on the model parameters. This relationship can be expressed explicitly as:

$$\mathbf{Y}_t = \mathbf{A}(L) \mathbf{S}_t = \mathbf{A}(L) (\mathbf{I} - \mathbf{\Theta}_1 L)^{-1} [\mathbf{\Theta}_\varepsilon, \mathbf{\Theta}_\epsilon] \begin{pmatrix} \boldsymbol{\varepsilon}_t \\ \boldsymbol{\epsilon}_t \end{pmatrix} \equiv \mathbf{H}(L, \boldsymbol{\gamma}) \begin{pmatrix} \boldsymbol{\varepsilon}_t \\ \boldsymbol{\epsilon}_t \end{pmatrix}, \quad (15)$$



where  $H(L, \gamma)$  depends on the lag operator  $L$  and the parameter vector  $\gamma$ . This formulation highlights how the observables  $\mathbf{Y}_t$  relate to structural and sunspot shocks through the dynamic propagation implied by the DSGE model.

Following [Qu and Tkachenko \(2012, 2017\)](#), the spectral density of  $\mathbf{Y}_t$  is uniquely given by:

$$\mathbf{f}_\gamma(\omega) = \frac{1}{2\pi} \mathbf{H}(e^{-i\omega}; \gamma) \boldsymbol{\Sigma}(\gamma) \mathbf{H}(e^{-i\omega}; \gamma)', \quad (16)$$

where  $\omega \in [-\pi, \pi]$  and  $\boldsymbol{\Sigma}(\gamma)$  denotes the covariance matrix of shocks:

$$\boldsymbol{\Sigma}(\gamma) = \begin{pmatrix} \mathbf{I} & \mathbf{0} \\ \mathbf{M} & \mathbf{I} \end{pmatrix} \begin{pmatrix} \boldsymbol{\Sigma}_\varepsilon & \mathbf{0} \\ \mathbf{0} & \boldsymbol{\Sigma}_\epsilon \end{pmatrix} \begin{pmatrix} \mathbf{I} & \mathbf{M} \\ \mathbf{0} & \mathbf{I} \end{pmatrix}^\top. \quad (17)$$

In the determinacy case, sunspot shocks do not affect the solution, and hence  $\boldsymbol{\Theta}_\epsilon = \mathbf{0}$ . Consequently,  $\boldsymbol{\Sigma}(\gamma)$  reduces to  $\boldsymbol{\Sigma}_\varepsilon$ .

## 3.2 Identification under determinacy

In this subsection, I examine the identification properties of the parameter vector at the posterior mean of the DSGE model. The posterior mean is estimated using Bayesian estimation with SMC sampling.

### 3.2.1 Data

Since [L’Huillier et al. \(2024\)](#) provides Bayesian estimation results with MCMC sampling exclusively for medium-scale DSGE models, I conduct Bayesian estimation for the small-scale model using quarterly U.S. data. Following [Qu and Tkachenko \(2017\)](#), I divide the dataset into two periods: the Pre-Volcker period (1960Q1 to 1979Q2) and the Post-1982 period (1982Q4 to 1997Q4). The former period is used to estimate the model under indeterminacy, while the latter corresponds to the determinacy case. I use the same data as [Smets and Wouters \(2007\)](#), with three observable variables: output growth, inflation, and the interest rate. Since my focus is not on estimating steady-state parameters, I demean these observables so that  $(\hat{y}_t - \hat{y}_{t-1}, \hat{\pi}_t, \hat{i}_t)$  are centered around the steady state  $(0, 0, 0)$ . The

observation equation can thus be written as:

$$YGR_t = \hat{y}_t - \hat{y}_{t-1}$$

$$INFL_t = \hat{\pi}_t$$

$$INT_t = \hat{r}_t,$$

where  $YGR_t$  is the quarterly GDP growth rate,  $INFL_t$  is quarterly inflation rate and  $INT_t$  is the quarterly nominal interest rate.

### 3.2.2 Bayesian estimation with SMC sampling

In this paper, I estimate the small-scale DSGE model using Bayesian methods with SMC sampling, which serves as a benchmark for my identification analysis. SMC provides an alternative approach to sampling from the posterior distribution compared to traditional MCMC methods. Rather than relying on a single long chain with an initial burn-in period, SMC gradually transforms a set of weighted particles from the prior distribution into the posterior distribution by passing through a sequence of bridge distributions. At each stage, particles are reweighted, resampled to prevent degeneracy, and propagated via a Markov transition kernel to adapt to the current bridge distribution. As demonstrated by [Herbst and Schorfheide \(2014\)](#), SMC is less noisy, more efficient, and yields higher estimation precision than the Random Walk Metropolis-Hastings (RWMH) algorithm, a commonly used MCMC technique. Additionally, SMC performs significantly better with multimodal posterior distributions, as it samples from multiple modal regions with greater precision. This capability is crucial when estimating parameters related to nominal and wage rigidity, whose posterior distributions often exhibit multimodal characteristics. Although not the primary focus of this paper, SMC also exhibits superior performance when employing diffuse priors, making it particularly suitable for situations with limited prior information.

The prior distributions selected are summarized in Table 1. The prior means for  $\theta$ ,  $\phi_y$ ,  $\phi_\pi$ , and  $\kappa$  align with the calibrations used by [L’Huillier et al. \(2024\)](#). Additionally, following [L’Huillier et al. \(2024\)](#), I calibrate discount factor  $\beta = 0.99$  and inverse Frisch elasticity  $\nu = 2^3$ . As discussed earlier, due to the multimodal nature of the Phillips Curve

---

<sup>3</sup>I calibrate  $\beta$  because the data has been demeaned. Since the model is locally identified only when  $\nu$  is fixed, even under RE, I set  $\nu = 2$ . My primary objective is to test whether DE can be identified, rather than to

Table 1: Prior and Posterior Distributions

Param.	Prior				Posterior DE		Posterior RE	
	Description	Dist.	Mean	Std.	Mean	[05, 95]	Mean	[05, 95]
$\theta$	diagnosticity	Normal	1.00	0.30	0.57	[0.41, 0.74]	0	—
$\phi_y$	m.p. rule	Normal	0.50	0.25	0.11	[0.07, 0.14]	0.08	[0.05, 0.11]
$\phi_\pi$	m.p. rule	Normal	1.50	0.25	1.15	[0.99, 1.31]	1.21	[0.99, 1.38]
$\kappa$	P.C. slope	Gamma	0.05	0.025	0.12	[0.08, 0.16]	0.15	[0.10, 0.20]
$\rho_a$	persis. tech.	Beta	0.50	0.20	0.77	[0.65, 0.91]	0.56	[0.41, 0.74]
$\rho_g$	persis. fisc.	Beta	0.50	0.20	0.93	[0.91, 0.96]	0.95	[0.94, 0.97]
$\sigma_a$	s.d. tech.	Inv. Gamma	0.50	1.00	0.61	[0.38, 0.83]	0.91	[0.60, 1.23]
$\sigma_g$	s.d. fisc.	Inv. Gamma	0.50	1.00	1.79	[1.42, 2.15]	1.54	[1.31, 1.80]
$\sigma_m$	s.d. mon.	Inv. Gamma	0.50	1.00	0.38	[0.33, 0.44]	0.39	[0.33, 0.46]

Note: The results were estimated using Dynare version 6.2, with the number of particles ( $N$  in [Herbst and Schorfheide \(2014\)](#)) set to 3,000 and the number of stages ( $N_\phi$  in [Herbst and Schorfheide \(2014\)](#)) set to 200. The parameter  $\lambda$  is set to 2, with an initial scaling parameter of 0.5 and an initial acceptance rate of 0.25. These settings align with those used by [Cai et al. \(2021\)](#) in the Bayesian SMC estimation for [An and Schorfheide \(2007\)](#). Since [Cai et al. \(2021\)](#) demonstrated that the gain from increasing the mutation block is limited, I set it to 1.

(PC) slope parameter, the prior for  $\kappa$ , which is inversely related to price rigidity, plays a significant role in its estimation. According to [Del Negro and Schorfheide \(2008\)](#), two competing views exist regarding price rigidity: one favoring high rigidity and the other low rigidity. Evaluating these perspectives is beyond the scope of this paper; therefore, I adopt a high price rigidity prior consistent with the calibration in [L’Huillier et al. \(2024\)](#), which is supported by extensive literature (e.g., [Schorfheide 2008](#); [Nakamura and Steinsson 2014](#); [Galí 2015](#); [Jones et al. 2021](#); [Hazell et al. 2022](#)). The shock-related priors used are standard. I employ Dynare 6.2 for the SMC Bayesian estimation. Table 2 reports the posterior mean estimates along with their 90% credible intervals. For the subsequent identification analysis, I use the posterior means of both DE and RE models as the respective  $\gamma_0$  values.

### 3.2.3 Local identification

In the context of spectrum analysis, the parameter vector  $\gamma$  is locally identifiable from the second order properties of  $\{Y_t\}$  at a point  $\gamma_0$  refers to the existing of an open neighborhood

---

assess the model’s overall identification or fit to the data.

of  $\gamma_0$  such that

$$f_{\gamma_0}(\omega) = f_{\gamma_1}(\omega), \forall \omega \in [-\pi, \pi] \Leftrightarrow \gamma_0 = \gamma_1.$$

As established by Theorem 1 in [Qu and Tkachenko \(2012\)](#), a necessary and sufficient condition for second-order identification at  $\gamma_0$  is that

$$G(\gamma_0) = \int_{-\pi}^{\pi} \left( \frac{\partial \text{vec} f_{\gamma_0}(\omega)}{\partial \gamma'} \right)' \left( \frac{\partial \text{vec} f_{\gamma_0}(\omega)}{\partial \gamma'} \right) d\omega \quad (18)$$

must has full rank, where operator *vec* vectorizes a matrix by stacking its columns. Note that this condition also holds in the time domain. I use the spectrum domain version to stay in line with Qu and Tkachenko's structure.<sup>4</sup> The  $(j, k)$ th element of  $G$ -matrix is

$$G_{jk}(\gamma) = \int_{-\pi}^{\pi} \text{tr} \left\{ \frac{\partial \text{vec} f_{\gamma}(\omega)}{\partial \gamma_j} \frac{\partial \text{vec} f_{\gamma}(\omega)}{\partial \gamma_k} \right\} d\omega$$

In practice, both integrals and derivatives can be computed numerically using the algorithm described in [Qu and Tkachenko \(2012\)](#)<sup>5</sup>. The frequency interval  $[-\pi, \pi]$  is partitioned into  $N$  subintervals, and derivatives are approximated using the two-point finite difference method:

$$\frac{f_{\gamma_0 + \mathbf{e}_j h_j}(\omega_s) - f_{\gamma_0}(\omega_s)}{h_j}, \quad j = 1, \dots, N + 1,$$

where  $\omega_s$  is sth frequency in partition,  $\mathbf{e}_j$  is a unit vector with  $j$ th element equals to 1 and  $h_j$  is the step size. The integral can be approximated by Riemann sum

$$\frac{2\pi}{N + 1} \sum_{s=1}^{N+1} \text{tr} \left\{ \frac{\partial f_{\gamma}(\omega_s)}{\partial \gamma_j} \frac{\partial f_{\gamma}(\omega_s)}{\partial \gamma_k} \right\}.$$

Under rational expectations, with parameter vector  $\gamma_0^{RE} = [\phi_y, \phi_{\pi}, \beta, \kappa, \rho_a, \rho_g, \sigma_a, \sigma_g, \sigma_m]$  = [0.08, 1.21, 0.99, 0.15, 0.56, 0.95, 0.91, 1.54, 0.39], the  $G$ -matrix has full rank, and its eigenvalues are [189.9564, 1.0621, 0.6920, 0.3156, 0.0218, 0.0130, 0.0003, 0.0015, 0.0025]. Similarly, under diagnostic expectations, with parameter vector  $\gamma_0^{DE} = [\theta, \phi_y, \phi_{\pi}, \beta, \kappa, \rho_a, \rho_g, \sigma_a, \sigma_g, \sigma_m]$  = [0.57, 0.11, 1.15, 0.99, 0.12, 0.77, 0.93, 0.61, 1.79, 0.38], the  $G$ -matrix

<sup>4</sup>The time domain version of this condition see [Iskrev \(2010\)](#)'s full column rank condition of the Jacobian matrix.

<sup>5</sup>The numerical computations are implemented in the Matlab code *G\_computation.m* provided by [Qu and Tkachenko \(2012\)](#).

also has full rank, with eigenvalues [185.2036, 1.7322, 0.8938, 0.4829, 0.0874, 0.0275, 0.0236, 0.0149, 0.0043, 0.0017]. Therefore, our example small-scale DSGE model is locally identified based on the second-order properties of  $\{Y_t\}$  at both  $\gamma_0^{RE}$  and  $\gamma_0^{DE}$ .

### 3.2.4 Global identification

The parameter vector  $\gamma$  is said to be globally identifiable from the second-order properties of  $\{Y_t\}$  at  $\gamma_0$  if and only if, within the parameter space  $\Theta$ , ,

$$f_{\gamma_0}(\omega) = f_{\gamma_1}(\omega), \quad \forall \omega \in [-\pi, \pi] \Leftrightarrow \gamma_0 = \gamma_1.$$

Theorem 2 in [Qu and Tkachenko \(2017\)](#) establishes that, under certain assumptions<sup>6</sup>,  $\gamma$  is globally identifiable from the second-order properties of  $Y_t$  if and only if the KL distance between two DSGE models is positive for any  $\gamma_1 \in \Theta$  with  $\gamma_1 \neq \gamma_0$ . The KL distance writes

$$KL(\gamma_0, \gamma_1) = \frac{1}{4\pi} \int_{-\pi}^{\pi} \{tr(\mathbf{f}_{\gamma_1}^{-1}(\omega)\mathbf{f}_{\gamma_0}(\omega)) - \logdet((\mathbf{f}_{\gamma_1}^{-1}(\omega)\mathbf{f}_{\gamma_0}(\omega)) - n_Y)\}d\omega, \quad (19)$$

where  $n_Y$  is the dimension of  $Y_t(\gamma)$ . If the DSGE model is locally identified at  $\gamma_0$ , the global identification condition can be further reduced to checking

$$\inf_{\gamma_1 \in \Theta \setminus B(\gamma_0)} KL(\gamma_0, \gamma_1) > 0 \quad (20)$$

, where  $B(\gamma_0)$  is an open neighbourhood of  $\gamma_0$ .

In practice, the KL distance is calculated numerically and hence subject to accuracy error from three aspects. First, the solution of DSGE in this paper is calculated using Sims' Matlab file *gensys.m* with an error rate of order 1E-15([Anderson, 2008](#)). Second, similar to the local identification case, there is an approximation error for the integral. Third, the minimization of KL distance is up to some tolerance level. Therefore, [Qu and Tkachenko \(2017\)](#) proposes to regard KL as zero when KL is smaller than 1E-10. Later, they develop three methods to find evidence contradicting the conclusion. In this paper, I focus on one of these three methods, i.e., empirical KL distance measure.

In short, the empirical KL distance can be interpreted as the rejection probability of a

---

<sup>6</sup>See Assumptions 1, 2, and 4 in [Qu and Tkachenko \(2017\)](#).

likelihood ratio type test based on  $T$  hypothetical sample observations. In the context of global identification, the null hypothesis states that  $f_{\gamma_0}(\omega)$  is the true spectral density, while the alternative hypothesis posits that  $f_{\gamma_c}(\omega)$  is the true spectral density, where  $\gamma_c$  denotes the parameter vector that minimizes the KL divergence over the feasible parameter space, excluding a neighborhood of  $\gamma_0$  of size  $c$ . The corresponding test statistic asymptotically follows a normal distribution with variance determined by the assumed true model.<sup>7</sup> The empirical KL distance thus reflects the probability that the two models differ in a statistically detectable way. Setting the significance level at 5%, if the empirical KL distance exceeds 5% and increases with the sample size  $T$ , we conclude that the DSGE model is globally identified.

Table 2: Parameter values minimizing the KL criterion, HSY (2024) model under RE

	(a) All parameters can vary				(b) $\beta(\phi_\pi$ for $c = 1$ ) fixed			(c) $\beta \& \phi_\pi$ ( $\phi_\pi \& \sigma_a$ ) fixed		
	$\gamma_0^{RE}$	$c = 0.1$	$c = 0.5$	$c = 1$	$c = 0.1$	$c = 0.5$	$c = 1$	$c = 0.1$	$c = 0.5$	$c = 1$
$\phi_y$	0.08	0.08	0.08	0.13	0.09	0.04	0.04	0.08	0.06	0.05
$\phi_\pi$	1.21	1.18	1.09	<b>0.21</b>	<b>1.11</b>	<b>1.71</b>	1.21	1.21	1.21	1.21
$\beta$	0.99	<b>0.89</b>	<b>0.49</b>	0.35	0.99	0.99	0.10	0.99	0.99	0.999
$\kappa$	0.15	0.15	0.16	0.10	0.13	0.26	0.12	0.13	0.09	0.14
$\rho_a$	0.56	0.56	0.55	0.57	0.56	0.52	0.53	0.55	0.52	0.60
$\rho_g$	0.95	0.95	0.94	0.91	0.95	0.95	0.94	0.95	0.96	0.97
$\sigma_a$	0.91	0.98	1.20	1.77	0.98	0.77	<b>1.91</b>	<b>1.01</b>	<b>1.41</b>	0.91
$\sigma_g$	1.54	1.48	1.30	1.17	1.54	1.54	1.08	1.54	1.57	<b>2.54</b>
$\sigma_m$	0.39	0.39	0.38	0.38	0.39	0.41	0.39	0.39	0.39	0.38

Note: KL denotes  $KL_{ff}(\gamma_0, \gamma_c)$  with  $\gamma_0$  corresponding to the benchmark specification. The values are rounded to the second decimal place except for  $\beta$ . The bold value signifies the binding constraint.

I use the replication code from [Qu and Tkachenko \(2017\)](#) to minimize  $KL(\gamma_0^{RE}, \gamma^{RE})$  under the constraint  $\|\gamma^{RE} - \gamma_0^{RE}\|_\infty \geq c$  for the benchmark RE model. The results are presented in Tables 2 and 3. When all parameters are allowed to vary, the KL distance is relatively small, but remaining above  $1 \times 10^{-10}$ . For small sample periods, the empirical KL distance is slightly below 0.05, increasing to just above 0.05 as  $T$  exceeds 200. This suggests that the model exhibits challenges in distinguishing with limited sample sizes. Notably, the parameter  $\beta$  binds the constraint for neighborhood sizes of 0.1 and 0.5<sup>8</sup>, while  $\phi_\pi$  binds it for

<sup>7</sup>For the formal result, see Theorem 3 in [Qu and Tkachenko \(2017\)](#).

<sup>8</sup>See the bold numbers in Table 3.

Table 3: KL and empirical distances between  $\gamma_c$  and  $\gamma_0$ , HSY (2024) model under RE

	<b>(a) All parameters can vary</b>			<b>(b) <math>\beta(\phi_\pi</math> for <math>c = 1</math>) fixed</b>			<b>(c) <math>\beta \&amp; \phi_\pi(\phi_\pi \&amp; \sigma_a)</math> fixed</b>		
	$c = 0.1$	$c = 0.5$	$c = 1$	$c = 0.1$	$c = 0.5$	$c = 1$	$c = 0.1$	$c = 0.5$	$c = 1$
KL	5.06E-05	1.45E-03	0.0160	3.59E-04	1.31E-02	0.0202	0.0011	0.0155	0.1389
$T = 80$	0.0463	0.0501	0.2449	0.0824	0.3662	0.5231	0.1213	0.5434	0.9827
$T = 150$	0.0497	0.0730	0.4744	0.0966	0.5810	0.7507	0.1551	0.7393	0.9989
$T = 200$	0.0516	0.0894	0.6161	0.1055	0.6978	0.8489	0.1770	0.8280	0.9998
$T = 1000$	0.0730	0.3677	0.9999	0.2165	0.9997	0.9999	0.4542	0.9999	1.0000

Note: KL denotes  $KL_{ff}(\gamma_0, \gamma_c)$  with  $\gamma_0$  given in the columns of Table 2. The empirical distance measure equals  $p_{ff}(\gamma_0, \gamma_c, 0.05, T)$ , where T is specified in the last four rows of the table.

a neighborhood size of 1. This difference arises from setting the bound for  $\beta$  to  $[0.1, 0.999]$  to maintain economic interpretability, which prevents  $\beta$  from binding the constraint for a neighborhood size of 1. Thus, the results indicate that the discount factor plays a significant role in the difficulty of achieving global identification, with the monetary policy response coefficient to inflation likely being the next most influential factor.

Next, I fix the "problematic" parameter  $\beta$  (and  $\phi_\pi$  for a neighborhood size of 1) and search for the remaining parameters that minimize the KL distance. This adjustment yields a significant improvement, with the empirical KL distance exceeding 0.05 even for a small sample period,  $T = 80$ , across all neighborhood sizes. For  $c = 0.5$  and  $T = 150$ , the empirical distance reaches 0.5810 (0.7507 for  $c = 1$  and  $T = 150$ ). During this process,  $\phi_\pi$  ( $\sigma_a$ ) binds the constraint, indicating that it is the second (third) most influential parameter contributing to failure of global identification. I then fix  $\phi_\pi$  ( $\sigma_a$ ) and repeat the analysis, resulting in further substantial improvement. The empirical distance is 0.7393 for  $c = 0.5$  (0.9989 for  $c = 1$ ) and  $T = 150$ , with  $\sigma_a$  ( $\sigma_g$ ) binding the constraint.

Similarly, I conduct the identification exercise by minimizing the KL divergence  $KL(\gamma_0^{DE}, \gamma^{DE})$  under the constraint  $\|\gamma^{DE} - \gamma_0^{DE}\|_\infty \geq c$  for the benchmark model with DE. The results, shown in Tables 4 and 5, indicate that when all parameters vary, the empirical KL distances consistently exceed 0.05 and increase with sample size  $T$ , implying no observational equivalence. While direct comparison of absolute KL values between the RE and DE models is not meaningful due to the additional DE parameter, examining the relative identification strength of individual parameters reveals important insights.

Table 4: Parameter values minimizing the KL criterion, HSY (2024) model under DE

	(a) All parameters can vary				(b) $\sigma_a$ fixed			(c) $\sigma_a$ and $\sigma_g$ fixed		
	$\gamma_0^{DE}$	$c = 0.1$	$c = 0.5$	$c = 1$	$c = 0.1$	$c = 0.5$	$c = 1$	$c = 0.1$	$c = 0.5$	$c = 1$
$\theta$	0.57	0.63	0.81	0.38	0.61	0.38	0.21	0.55	0.53	0.51
$\phi_y$	0.11	0.11	0.12	0.13	0.11	0.14	0.09	0.10	0.06	0.01
$\phi_\pi$	1.15	1.07	0.73	0.38	1.13	1.11	1.07	<b>1.25</b>	<b>1.65</b>	<b>2.15</b>
$\beta$	0.990	0.902	0.686	0.620	0.958	0.966	0.999	0.999	0.999	0.999
$\kappa$	0.12	0.11	0.09	0.07	0.12	0.13	0.14	0.14	0.23	0.34
$\rho_a$	0.77	0.76	0.76	0.72	0.77	0.83	0.75	0.74	0.67	0.60
$\rho_g$	0.93	0.93	0.91	0.91	0.93	0.89	0.95	0.93	0.93	0.93
$\sigma_a$	0.61	<b>0.71</b>	<b>1.11</b>	<b>1.61</b>	0.61	0.61	0.61	0.61	0.61	0.61
$\sigma_g$	1.79	1.71	1.54	1.41	<b>1.69</b>	<b>1.29</b>	<b>2.79</b>	1.79	1.79	1.79
$\sigma_m$	0.38	0.38	0.37	0.37	0.38	0.39	0.37	0.38	0.39	0.44

Note: KL denotes  $KL_{ff}(\gamma_0, \gamma_c)$  with  $\gamma_0$  corresponding to the benchmark specification. The values are rounded to the second decimal place except for  $\beta$ . The bold value signifies the binding constraint.

Table 5: KL and empirical distances between  $\gamma_c$  and  $\gamma_0$ , HSY (2024) model

	(a) All parameters can vary			(b) $\sigma_a$ fixed			(c) $\sigma_a$ and $\sigma_g$ fixed		
	$c = 0.1$	$c = 0.5$	$c = 1$	$c = 0.1$	$c = 0.5$	$c = 1$	$c = 0.1$	$c = 0.5$	$c = 1$
KL	2.15E-04	5.16E-03	1.23E-02	8.05E-04	0.0266	0.0811	1.50E-03	0.0378	0.1230
$T = 80$	0.0565	0.1540	0.3232	0.0823	0.5232	0.9727	0.1077	0.6653	0.9794
$T = 150$	0.0649	0.2515	0.5267	0.1048	0.7857	0.9983	0.1457	0.9154	0.9999
$T = 200$	0.0701	0.3196	0.6438	0.1196	0.8873	0.9998	0.1712	0.9725	1.0000
$T = 1000$	0.1346	0.9167	0.9992	0.3222	1.0000	1.0000	0.5092	1.0000	1.0000

Note: KL denotes  $KL_{ff}(\gamma_0, \gamma_c)$  with  $\gamma_0$  given in the columns of Table 5. The empirical distance measure equals  $p_{ff}(\gamma_0, \gamma_c, 0.05, T)$ , where T is specified in the last four rows of the table.

Under DE, the shock variance parameters  $\sigma_a$  and  $\sigma_g$  exhibit the weakest identification strength, followed by  $\phi_\pi$ . As shown in L’Huillier et al. (2024)’s online appendix<sup>9</sup>, the DE parameter  $\theta$  influences the policy functions solely through the shock terms. Consequently, introducing  $\theta$  effectively redistributes the explanatory power of shocks on endogenous variables, which reduces the curvature of the model implied spectrum to changes in shock variances. Intuitively, since  $\theta$  modulates how shocks propagate into the system, variations in the underlying shock variances produce smaller changes in the observable spectral proper-

<sup>9</sup>See also the analytical solution to the modified model in Appendix section 6.1.



ties. This reduction in spectral sensitivity translates into weaker identification for  $\sigma_a$  and  $\sigma_g$ . Despite this, the model remains globally identifiable under DE, with the DE parameter  $\theta$  itself demonstrating relatively strong identification.

### 3.2.5 Robustness check: Identification of parameters estimated via MCMC Bayesian

This subsection provides a robustness check on the identification properties of the diagnostic parameter  $\theta$  by examining identification under an alternative set of parameters estimated using Bayesian MCMC. The priors are the same as those used for the Bayesian SMC estimation, shown in Table 1, and the posterior distribution obtained via Bayesian MCMC is presented in Table 6.

Table 6: Posterior Distribution

Parameter	Mean	[05, 95]
$\theta$	0.56	[0.44, 0.70]
$\phi_y$	0.10	[0.07, 0.13]
$\phi_\pi$	1.14	[1.00, 1.26]
$\kappa$	0.13	[0.08, 0.17]
$\rho_a$	0.80	[0.65, 0.91]
$\rho_g$	0.94	[0.92, 0.96]
$\sigma_a$	0.55	[0.39, 0.74]
$\sigma_g$	1.77	[1.49, 2.08]
$\sigma_m$	0.38	[0.33, 0.45]

Note: The results were estimated using Dynare version 6.2 with a type of MCMC, slice sampling. The number of replication draws is set to 700, which, according to Planas et al. (2015), is approximately equivalent to 50,000 draws using classical Metropolis-Hastings sampling. The number of replication blocks is set to 1.

The identification results are shown in Tables 7 and 8. This alternative set of parameters yields a similar identification profile, with the two lowest identification strength of the parameters matching the results obtained under SMC sampling. For the neighborhoods of  $c = 0.5$  and  $c = 1$ , the third parameter with the lowest identification strength becomes the diagnostic parameter. Despite this, the empirical KL distance is 0.7966, which is significantly larger than the threshold of 0.05 for a small sample size of  $T = 80$  in the neighborhood  $c = 0.5$ .

Therefore, it is valid to conclude that the diagnostic parameter  $\theta$  is robustly identified.

Table 7: Parameter values minimizing the KL criterion, HSY (2024) model under DE

	(a) All parameters can vary				(b) $\sigma_a$ fixed			(c) $\sigma_a$ and $\sigma_g$ fixed		
	$\gamma_0^{MCMC}$	$c = 0.1$	$c = 0.5$	$c = 1$	$c = 0.1$	$c = 0.5$	$c = 1$	$c = 0.1$	$c = 0.5$	$c = 1$
$\theta$	0.56	0.61	0.76	0.84	0.60	0.47	0.42	0.58	<b>0.06</b>	<b>1.56</b>
$\phi_y$	0.10	0.10	0.11	0.11	0.11	0.09	0.09	0.11	0.09	0.18
$\phi_\pi$	1.14	1.06	0.75	0.38	1.13	1.12	1.10	<b>1.04</b>	1.07	0.68
$\beta$	0.990	0.894	0.644	0.502	0.966	0.999	0.999	0.974	0.999	0.72
$\kappa$	0.13	0.12	0.10	0.07	0.14	0.12	0.11	0.11	0.20	0.13
$\rho_a$	0.80	0.80	0.79	0.78	0.81	0.81	0.83	0.82	0.74	0.87
$\rho_g$	0.94	0.94	0.93	0.92	0.94	0.95	0.95	0.94	0.95	0.83
$\sigma_a$	0.55	<b>0.65</b>	<b>1.05</b>	<b>1.55</b>	0.55	0.55	0.55	0.55	0.55	0.55
$\sigma_g$	1.77	1.70	1.54	1.48	<b>1.67</b>	<b>2.27</b>	<b>2.77</b>	1.77	1.77	1.77
$\sigma_m$	0.38	0.38	0.37	0.37	0.38	0.38	0.38	0.38	0.37	0.39

Note: KL denotes  $KL_{ff}(\gamma_0^{MCMC}, \gamma_c^{MCMC})$  with  $\gamma_0^{MCMC}$  corresponding to the benchmark specification. The values are rounded to the second decimal place except for  $\beta$ . The bold value signifies the binding constraint.

Table 8: KL and empirical distances between  $\gamma_c$  and  $\gamma_0$ , HSY (2024) model

	(a) All parameters can vary			(b) $\sigma_a$ fixed			(c) $\sigma_a$ and $\sigma_g$ fixed		
	$c = 0.1$	$c = 0.5$	$c = 1$	$c = 0.1$	$c = 0.5$	$c = 1$	$c = 0.1$	$c = 0.5$	$c = 1$
KL	1.15E-04	2.51E-03	6.94E-03	9.19E-04	0.0224	0.0718	2.09E-03	0.0385	0.1541
$T = 80$	0.0535	0.0964	0.1912	0.0856	0.7032	0.9664	0.1689	0.7966	0.9982
$T = 150$	0.0592	0.1451	0.3184	0.1106	0.8739	0.9975	0.2262	0.9552	0.9999
$T = 200$	0.0627	0.1794	0.4044	0.1270	0.9327	0.9996	0.2635	0.9860	1.0000
$T = 1000$	0.1032	0.6467	0.9701	0.3536	1.0000	1.0000	0.6784	1.0000	1.0000

Note: KL denotes  $KL_{ff}(\gamma_0^{MCMC}, \gamma_c^{MCMC})$  with  $\gamma_0^{MCMC}$  given in the columns of Table 8. The empirical distance measure equals  $p_{ff}(\gamma_0^{MCMC}, \gamma_c^{MCMC}, 0.05, T)$ , where T is specified in the last four rows of the table.

The practical differences between the estimation methods can arise due to the computational characteristics and sampling efficiencies of each. For example, SMC dynamically resamples the parameter space and can be more effective in multimodal regions, which may make it more sensitive to the weak identification of certain parameters. In contrast, MCMC operates differently in exploring parameter space and might identify other parameters as

weakly identified due to broader credible intervals in regions with flat likelihoods. Thus, while global identification ensures a unique parameter structure, numerical and sampling variations between SMC and MCMC can reveal different aspects of identification precision, highlighting certain parameters with varying degrees of weakness depending on the estimation method used.

### 3.3 Identification under indeterminacy

Qu and Tkachenko (2017) show that certain parameters are identifiable under indeterminacy but not under determinacy. Moreover, L’Huillier et al. (2024) argue that the relative strength of the central bank’s policy response versus diagnostic distortions determines the size of the fiscal multiplier. Indeterminacy typically arises under a dovish monetary policy, when the policy reaction coefficient to inflation is below one. Estimation in the indeterminacy region therefore provides a distinctive empirical setting to study the interaction between monetary policy and DE. Motivated by this, I examine the identification of the diagnostic parameter in the indeterminacy case as a robustness check. Since Dynare’s Bayesian estimation routines are restricted to the determinacy case, I extend the SMC framework of Herbst and Schorfheide (2014) by incorporating the indeterminacy solution method of Lubik and Schorfheide (2004), thereby enabling SMC-based Bayesian estimation of DSGE models under indeterminacy.

The SMC algorithm itself proceeds as briefly described above in Section 3.2.2. The only modification required for the indeterminacy case is to rewrite the DSGE model in state space form using the method of Lubik and Schorfheide (2004), which then feeds into the Kalman filter for likelihood evaluation. Specifically, I adjust the DSGE system in Equation 11 by adding the identity equation  $y_t = y_t$ , which accommodates the use of the growth rate observable  $\hat{y}_t - \hat{y}_{t-1}$ . This change alters the state vector in Sims’ canonical form while leaving the shock vectors unchanged. The transition equation becomes:

$$\mathbf{S}_t^e = \Theta_1^e \mathbf{S}_{t-1}^e + \mathbf{R} \mathbf{e}_t, \quad \mathbf{e}_t \sim \mathcal{N}(\mathbf{0}, \Sigma(\gamma)), \quad (21)$$

where  $\mathbf{S}_t^e = (\hat{y}_t, \hat{\pi}_t, P_t, X_t, Q_t, Y_t, \hat{i}_t, \hat{a}_t, \hat{g}_t, \hat{y}_{t-1})'$ ,  $\mathbf{e}_t = [\boldsymbol{\varepsilon}_t, \boldsymbol{\epsilon}_t]'$ , and  $\mathbf{R} = [\Theta_\varepsilon^e, \Theta_\epsilon^e]$ . The super-

script “e” denotes the settings used for estimation. The measurement equation is:

$$\mathbf{Y}_t^e = \mathbf{A}^e \mathbf{S}_t^e, \quad (22)$$

with no measurement error included. The selection matrix  $\mathbf{A}^e$  and the explicit augmented Sims canonical form matrices  $\mathbf{\Gamma}_0^e$ ,  $\mathbf{\Gamma}_1^e$ ,  $\mathbf{\Psi}^e$ , and  $\mathbf{\Pi}^e$  are provided in Online Appendix. The coefficient matrices  $\mathbf{\Theta}_1^e$  and  $\mathbf{R}$  are computed numerically using the modified code *gensys\_mod.m* from [Qu and Tkachenko \(2017\)](#), based on Sims’ original *gensys.m*.

The prior distributions and posterior results for the indeterminacy case are reported in Table 9. Relative to the determinacy estimation, monetary policy places less weight on inflation ( $\phi_\pi = 0.36$ ) and more weight on the output gap. The data also favor a more persistent and more volatile TFP process, while the government spending process becomes less persistent and less volatile. This pattern is consistent with [L’Huillier et al. \(2024\)](#), who show that if the diagnostic parameter exceeds the policy response coefficient, the fiscal multiplier can rise above one. In this case,  $\theta = 0.54$  is larger than  $\phi_\pi = 0.36$ , so only a modest government spending process is needed to generate realistic dynamics.<sup>10</sup>

Applying the identification checks under indeterminacy, the results are reported in Table 10 and Table 11. No observable equivalence is detected. The least well-identified parameters remain those related to shock variances and the monetary policy response to inflation. The weakest identified parameter is the projection coefficient of the sunspot shock onto the monetary policy shock, followed by the variance of government spending shocks, the monetary policy response to inflation, the time discount factor and the variance of TFP shocks. This pattern is intuitive: under DE, a dovish  $\phi_\pi$  and a large  $\sigma_g$  both generate strong output responses to government spending, thereby weakening their relative identification strength.

### 3.4 Detecting observable equivalence between DE and RE

In this subsection, I address the second research question of this paper: whether DE generate dynamics that are truly distinct from those under RE. To examine this, I follow

---

<sup>10</sup>The weak inflation response is also in line with the indeterminacy estimation literature. For example, [Qu and Tkachenko \(2017\)](#) estimate the rational expectations [An and Schorfheide \(2007\)](#) model with an interest rate smoothing rule and obtain posterior means of  $\psi_1 = 0.63$  and  $\rho_r = 0.87$ , which implies an effective inflation response  $(1 - \rho_r)\psi_1 \approx 0.1$ .

Table 9: Prior and Posterior Distributions

Parameter	Description	Distribution	Prior		Posterior	
			Mean	Std.dev	Mean	[05, 95]
$\theta$	diagnosticity	Normal	1	0.3	0.54	[0.26, 0.83]
$\phi_y$	m.p. rule	Normal	0.5	0.25	0.28	[0.20, 0.37]
$\phi_\pi$	m.p. rule	Normal	1.5	0.25	0.36	[0.16, 0.55]
$\kappa$	P.C. slope	Gamma	0.05	0.025	0.06	[0.03, 0.09]
$\rho_a$	persis. tech.	Beta	0.5	0.2	0.98	[0.95, 0.99]
$\rho_g$	persis. fisc.	Beta	0.5	0.2	0.78	[0.70, 0.86]
$\sigma_a$	s.d. tech.	Inv. Gamma	0.5	1	0.90	[0.74, 1.08]
$\sigma_g$	s.d. fisc.	Inv. Gamma	0.5	1	2.08	[1.59, 2.61]
$\sigma_m$	s.d. mon.	Inv. Gamma	0.5	1	0.30	[0.25, 0.35]
$M_{a\epsilon}$	proj. coeff.	Normal	0	1	0.58	[0.46, 0.71]
$M_{g\epsilon}$	proj. coeff.	Normal	0	1	0.21	[0.13, 0.30]
$M_{m\epsilon}$	proj. coeff.	Normal	0	1	-1.61	[-2.13, -1.11]
$\sigma_\epsilon$	s.d. sunspot	Inv. Gamma	0.5	1	0.34	[0.27, 0.43]

**Notes:** The inverse Gamma prior is given by  $p(\sigma \mid \iota, s) \propto \sigma^{-\iota-1} e^{-\frac{s^2}{2\sigma^2}}$ , where  $\iota = 4$  and  $s = 0.75$ . Posterior results were estimated using a modified MATLAB code from [Herbst and Schorfheide \(2016\)](#). All settings are consistent with the determinacy settings in Dynare: number of particles ( $N$ ) = 3,000, number of stages ( $N_\phi$ ) = 200,  $\lambda = 2$ , initial scaling parameter = 0.5, and initial acceptance rate = 0.25. Mutation block = 1. The modifications extend the algorithm to cover the indeterminacy region, manage random seeds deterministically across parallel workers to ensure fully reproducible results, and implement numerically stable weight updating via the log-sum-exp transformation to prevent overflow. The estimation results are robust to increasing the number of stages or particles, as well as to employing diffuse priors for the projection coefficient.

[Qu and Tkachenko \(2017\)](#) and [Qu and Tkachenko \(2023\)](#) and conduct an exercise based on an unconstrained minimization problem. Specifically, I fix the parameters of the benchmark DE model at their posterior means and then search for the parameter values of an alternative RE model to minimize the KL distance of the two spectra. In doing so, I impose  $\theta = 0$  for the RE model while allowing all other parameters to vary freely to minimize KL distance. This setup enables me to assess whether an RE framework can nevertheless replicate the dynamics generated under DE. I adopt the methodology of [Qu and Tkachenko \(2017\)](#) because, to the best of my knowledge, it remains the only approach that effectively addresses identification across different model structures which is helpful for assessing the role of  $\theta$  in shaping macroeconomic dynamics.

Table 10: Parameter values minimizing the KL criterion, HSY (2024) model under DE

	(a) All parameters can vary				(b) $M_{m\epsilon}$ fixed			(c) $M_{m\epsilon}$ and $\sigma_g$ fixed		
	$\gamma_0^{ind}$	$c = 0.1$	$c = 0.5$	$c = 1$	$c = 0.1$	$c = 0.5$	$c = 1$	$c = 0.1$	$c = 0.5$	$c = 1$
$\theta$	0.54	0.54	0.56	0.40	0.54	0.53	0.38	0.52	0.42	0.45
$\phi_y$	0.28	0.28	0.26	0.29	0.27	0.25	0.41	0.30	0.29	0.13
$\phi_\pi$	0.36	0.29	0.10	0.77	0.37	0.43	0.10	<b>0.26</b>	0.18	0.10
$\beta$	0.990	0.976	0.962	0.999	0.983	0.979	0.999	0.95	<b>0.49</b>	0.999
$\kappa$	0.06	0.06	0.04	0.20	0.06	0.07	0.06	0.07	0.26	0.01
$\rho_a$	0.98	0.98	0.98	0.98	0.98	0.98	0.98	0.98	0.98	0.97
$\rho_g$	0.78	0.78	0.77	0.82	0.79	0.83	0.67	0.78	0.81	0.83
$\sigma_a$	0.90	0.94	1.08	0.79	0.90	0.90	1.00	0.95	1.11	<b>1.90</b>
$\sigma_g$	2.08	2.08	2.14	2.12	<b>2.18</b>	<b>2.58</b>	<b>1.08</b>	2.08	2.08	2.08
$\sigma_m$	0.30	0.30	0.27	0.34	0.30	0.30	0.33	0.30	0.26	0.25
$\eta_a$	0.58	0.57	0.50	0.24	0.58	0.59	0.49	0.57	0.54	0.31
$\eta_g$	0.21	0.22	0.25	0.06	0.20	0.17	0.38	0.21	0.22	0.30
$\eta_m$	-1.61	<b>-1.71</b>	<b>-2.11</b>	<b>-0.61</b>	-1.61	-1.61	-1.61	-1.61	-1.61	-1.61
$s_\eta$	0.34	0.37	0.45	0.14	0.34	0.32	0.20	0.37	0.41	0.70

Note: KL denotes  $KL_{ff}(\gamma_0^{ind}, \gamma_c^{ind})$  with  $\gamma_0^{ind}$  corresponding to the benchmark specification. The values are rounded to the second decimal place except for  $\beta$ . The bold value signifies the binding constraint. Specifically,  $\phi_\pi$  varies within  $[0.1, 5]$ .

Table 11: KL and empirical distances between  $\gamma_c$  and  $\gamma_0$ , HSY (2024) model

	(a) All parameters can vary			(b) $M_{m\epsilon}$ fixed			(c) $M_{m\epsilon}$ and $\sigma_g$ fixed		
	$c = 0.1$	$c = 0.5$	$c = 1$	$c = 0.1$	$c = 0.5$	$c = 1$	$c = 0.1$	$c = 0.5$	$c = 1$
KL	5.76E-05	2.54E-03	0.0179	3.57E-04	7.42E-03	0.0687	1.53E-03	0.0270	0.0960
$T = 80$	0.0634	0.1707	0.5740	0.0918	0.4041	0.8491	0.1339	0.6996	0.9812
$T = 150$	0.0679	0.2347	0.7493	0.1068	0.5464	0.9913	0.1768	0.8715	0.9996
$T = 200$	0.0706	0.2768	0.8292	0.1162	0.6266	0.9992	0.2049	0.9310	1.0000
$T = 1000$	0.0999	0.7307	0.9998	0.2298	0.9870	1.0000	0.5517	1.0000	1.0000

Note: KL denotes  $KL_{ff}(\gamma_0^{ind}, \gamma_c^{ind})$  with  $\gamma_0^{ind}$  given in the columns of Table 8. The empirical distance measure equals  $p_{ff}(\gamma_0^{ind}, \gamma_c^{ind}, 0.05, T)$ , where T is specified in the last four rows of the table.

The results are presented in Tables 12 and 13. The search for minimizers is conducted over a relatively large parameter space:  $\gamma^{RE} = [\phi_y, \phi_\pi, \beta, \kappa, \rho_a, \rho_g, \sigma_a, \sigma_g, \sigma_m] \in [(0.1, 0.99); (0.1, 5); (0.1, 0.999); (0.01, 3); (0.1, 0.99); (0.1, 0.99); (0.1, 3); (0.1, 3); (0.1, 3)]$ . Despite the generous bounds on the parameter space, no set of parameters under RE produces spectra that closely resemble those of the DE model. The theoretical KL distance is 0.0711,

Table 12: Parameter values under DE and RE, HSY (2024) model

	DE	RE
$\theta$	0.57	0
$\phi_y$	0.11	0.09
$\phi_\pi$	1.15	1.19
$\beta$	0.99	0.999
$\kappa$	0.12	0.16
$\rho_a$	0.77	0.66
$\rho_g$	0.93	0.94
$\sigma_a$	0.61	0.79
$\sigma_g$	1.79	1.41
$\sigma_m$	0.38	0.37

Note: Column DE shows posterior means of parameters from the benchmark HYS (2024) model. Column RE shows parameters that minimize  $KL_{ff}(\gamma_0^{DE}, \gamma^{RE})$ , where  $f$  is the spectral density and  $\gamma^{RE}$  is the parameter vector under rational expectations.

Table 13: KL and empirical distances between DE and RE, HSY (2024) model

	Value
KL	0.0711
$T = 80$	0.9531
$T = 150$	0.9961
$T = 200$	0.9994
$T = 1000$	1.0000

Note: KL distance and the empirical distance measure are defined as  $KL_{fh}(\gamma_0^{DE}, \gamma^{RE})$  and  $p_{fh}(\gamma_0, \zeta, 0.05, T)$ , where  $h$  and  $\gamma^{RE}$  are the spectral density and structural parameter vector of the alternative model and  $T$  specified in the last four rows of the table.

and the empirical distance is larger than 0.9 even for  $T = 80$ . This provides strong evidence that DE plays a crucial role in generating macroeconomic dynamics, which cannot be replicated under rational expectations.

Interestingly, for the corresponding RE model to mimic the dynamics under DE, the spectrum favors less price rigidity, a less persistent but more volatile TFP process, and a slightly more persistent but less volatile government spending process. These results have clear economic intuition. Under DE, consumers extrapolate recent outcomes and demand responses are stronger, so prices adjust more sluggishly to accommodate these amplified

demand shifts. Similarly, agents extrapolate the effects of TFP shocks through their impact on output and inflation, making the aggregate responses appear more persistent than they actually are; the RE model mimics this by adopting a TFP process with higher volatility but lower persistence, producing comparable aggregate dynamics through different underlying mechanisms.

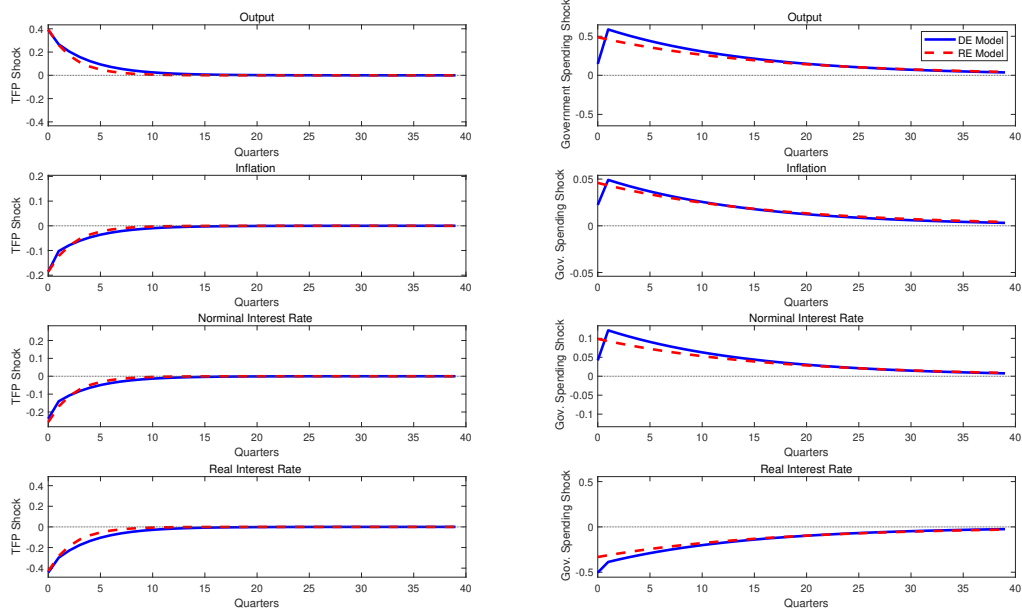
The government spending shock presents a particularly interesting case, as two distinct channels operate simultaneously. DE both extrapolates the spending shock itself and reduces the real interest rate through extrapolated inflation expectations (L’Huillier et al., 2024). Under a relatively dovish monetary policy rule where  $\phi_\pi < 2$ , the DE mechanism that lowers the real rate operates weakly. Consequently, the RE minimizer relies on only minor parameter adjustments: it raises the persistence of government spending shocks marginally, with  $\rho_g$  increasing from 0.93 to 0.94. Given the near unit root persistence, even this small increase substantially raises low frequency spectral power. To prevent the RE model from overshooting the DE dynamics, the minimizer compensates by reducing the variance of fiscal shocks, with  $\sigma_g$  falling from 1.79 to 1.41.

To illustrate this mechanism more intuitively, I plot the impulse responses for both the DE model and its closest RE counterpart, with parameters reported in Table 12. Following a positive TFP shock, output, inflation, and the nominal interest rate return to their steady states more quickly under RE than under DE. This occurs because the RE minimizer replicates DE’s extrapolation channel by choosing a TFP process with lower persistence but higher variance, which generates faster mean reversion through a different underlying mechanism.

As for the government spending shock, it reveals a fundamental difference between the two models that cannot be replicated through parameter adjustments alone. As shown in the bottom panel of the right column, the real interest rate falls much more sharply under DE than under RE following the spending shock. The reason is that agents with DE extrapolate inflation more strongly, which lowers the perceived real rate and amplifies demand through an expectation-driven channel. This produces a distinctive short-run “kick” in output and inflation that the RE model fundamentally cannot replicate, since it lacks this endogenous expectation amplification mechanism and must rely solely on exogenous parameter adjustments.



Figure 1: Impulse Responses: Comparing DE and RE models



Note: The panels show impulse responses of output, inflation, the nominal interest rate, and the real interest rate to a one standard deviation positive shock to TFP and government spending. The blue solid lines correspond to responses under DE, while the red dashed lines correspond to responses under RE. The RE parameters are chosen as the minimizers of the KL distance relative to the corresponding DE model (see Table 12).

Notably, the TFP shock does not exhibit the same distinctive “kick” in the real interest rate that characterizes the government spending shock. This difference arises from the structure of the model setup: TFP shock does not directly enter agents’ expectation formation process, appearing only in the output gap terms in both the Phillips curve and monetary policy rule. Consequently, while agents with DE still extrapolate the effects of productivity shocks through their impact on output and inflation, they do not directly extrapolate the TFP shock itself. In contrast, government spending shocks appear explicitly in agents’ expectations through the IS curve, creating a direct channel for expectation extrapolation that generates the amplified real interest rate response.

## 4 Identification analysis for a medium-scale DSGE

This section examines the global identification of the medium-scale DSGE model introduced by [L’Huillier et al. \(2024\)](#). Their specification extends the small-scale framework by incorporating several nominal, real, and informational frictions. Studying the medium-scale model serves two distinct purposes. First, it provides a setting to analyze whether DE remains identifiable once a broader set of frictions is present. Second, it enables an economic assessment of how these frictions interact with DE to shape model dynamics, clarifying which mechanisms are essential for reproducing empirically plausible macroeconomic behavior. I address these two questions separately in the subsections below.

### 4.1 Global identification

Specifically, [L’Huillier et al. \(2024\)](#) develop a standard medium-scale DSGE model that incorporates a wide range of frictions: investment adjustment costs, variable capital utilization, habit formation in consumption, price and wage stickiness, and noisy signals about permanent productivity. I follow their framework closely, with one key modification to the information structure. In their setting, following [Blanchard et al. \(2013\)](#), productivity consists of two components: a nonstationary permanent process and a stationary transitory process. Agents do not observe these components directly, but instead receive a noisy signal about the permanent component. In contrast, I work with a stationary system where the permanent productivity component is made stationary by expressing it in growth rates, and agents observe a noisy signal about the growth rate of permanent productivity. This modification is motivated by technical considerations. For the KL optimization, including the nonstationary permanent productivity level in the state vector produces a nearly flat objective function around zero frequency, leading to extremely slow convergence and numerical instability. Importantly, this adjustment is purely technical and does not alter the substantive economic interpretation of the information friction.

The model is driven by seven structural shocks: shocks to temporary and permanent productivity, a noise shock to signal about permanent productivity growth, a shock to the marginal efficiency of investment, price and wage markup shocks, and shocks to monetary and fiscal policy. In addition, the framework includes five measurement errors. These mea-

surement errors are introduced only to balance the number of shocks with the number of observables in the estimation and play no role in the identification analysis.

To estimate the model, L’Huillier et al. (2024) use 12 observables: output growth, consumption growth, investment growth, inflation, the interest rate, wage growth, labor growth, and one-period-ahead forecasts of output growth, consumption growth, investment growth, inflation, and the interest rate. However, as noted by Qu and Tkachenko (2023), global identification analysis requires the spectral density to be non-singular. Following Qu and Tkachenko (2023), I therefore work with log deviations from steady states of output, consumption, investment, wage, and labor, rather than their growth rates. Together with inflation and the interest rate, this yields 7 measurement variables in total. For completeness, Appendix 6.2 contains a detailed discussion of the modified information friction block as well as the full set of model equations.

Using the same approach as in the small-scale DSGE analysis, I take the posterior mean from Bayesian estimation as the benchmark parameter vector, denoted  $\gamma_0^{med}$ . Since the information-friction block is modified, I re-estimate the medium-scale model using standard MCMC sampling.<sup>11</sup> The full posterior results are reported in Table 14.

The global identification results are presented in Table 15 and 16<sup>12</sup>. When all parameters are allowed to vary, there is no evidence of observational equivalence. However, identification remains challenging with small sample sizes. The most problematic parameter is the shock variance  $\sigma_\mu$ , which exhibits the weakest identification<sup>13</sup>. I also conducted an identification exercise focusing exclusively on business cycle frequencies, which are the primary frequencies that DSGE models aim to study. This exercise is valuable for practitioners, as identification stemming from a potentially misspecified low-frequency component could provide misleading parameter estimates. The business cycle case results are largely similar to the full frequency case and shown in the Online Appendix.

---

<sup>11</sup>The resulting posterior distribution is very similar to that reported in Table 1 of L’Huillier et al. (2024), with the only notable difference being the variance of the noise shock, an expected outcome given that the signal now pertains to the growth rate rather than the level of permanent productivity.

<sup>12</sup>Local identification at  $\gamma_0^{med}$  has been verified but is not reported here for brevity.

<sup>13</sup>Under RE, it appears to be the second weakest identified parameter. Result are shown in Online Appendix.

Table 14: Posterior distribution

Parameter	Description	Post. Mean	90% HPD Interval
$\theta$	diagnosticity	0.72	[0.58, 0.86]
$\alpha$	cap. share	0.13	[0.12, 0.14]
$h$	habits	0.72	[0.70, 0.75]
$\frac{\chi''(1)}{\chi'(1)}$	cap. util. costs	5.09	[3.62, 6.55]
$\psi_p$	Rotemberg prices	122.47	[95.30, 148.26]
$\psi_w$	Rotemberg wages	507.44	[254.73, 773.38]
$\nu$	inv. Frisch elas.	3.71	[2.34, 5.05]
$S''(1)$	inv. adj. costs	6.93	[5.93, 7.99]
$\rho_R$	m.p. rule	0.58	[0.54, 0.62]
$\phi_\pi$	m.p. rule	1.54	[1.42, 1.66]
$\phi_x$	m.p. rule	0.006	[0.00, 0.01]
<i>Technology Shocks</i>			
$\rho$	persist.	0.85	[0.83, 0.87]
$\sigma_a$	tech. shock s.d.	1.43	[1.31, 1.55]
$\sigma_s$	noise shock s.d.	0.29	[0.23, 0.35]
<i>Investment-Specific Shocks</i>			
$\rho_\mu$	persist.	0.31	[0.25, 0.35]
$\sigma_\mu$	s.d.	18.63	[15.99, 21.82]
<i>Mark-up Shocks</i>			
$\rho_p$	persist.	0.88	[0.83, 0.92]
$\phi_p$	ma. comp.	0.58	[0.46, 0.70]
$\sigma_p$	s.d.	0.16	[0.13, 0.19]
$\rho_w$	persist.	0.997	[0.99, 1.00]
$\phi_w$	ma. comp.	0.54	[0.39, 0.66]
$\sigma_w$	s.d.	0.44	[0.35, 0.53]
<i>Policy Shocks</i>			
$\rho_{mp}$	persist.	0.03	[0.01, 0.05]
$\sigma_{mp}$	s.d.	0.38	[0.34, 0.42]
$\rho_g$	persist.	0.94	[0.91, 0.96]
$\sigma_g$	s.d.	0.37	[0.34, 0.40]
<i>Measurement Errors</i>			
$\sigma_{ygr}$	s.d.	0.50	[0.45, 0.55]
$\sigma_{cgr}$	s.d.	0.41	[0.36, 0.46]
$\sigma_{igr}$	s.d.	1.44	[1.26, 1.61]
$\sigma_\pi$	s.d.	0.27	[0.24, 0.30]
$\sigma_{\hat{i}}$	s.d.	0.16	[0.14, 0.18]

Note: This table shows the posterior distribution under DE. The values are rounded to two decimal places except for  $\phi_x$  and  $\rho_w$ .

Table 15: Parameter values minimizing the KL criterion, HSY (2024) model

	$\gamma_0^{med}$	(a) All parameters can vary			(b) $\sigma_\mu$ fixed		
		$c = 0.1$	$c = 0.5$	$c = 1.0$	$c = 0.1$	$c = 0.5$	$c = 1.0$
$\theta$	0.73	0.73	0.73	0.74	0.73	0.74	0.75
$\alpha$	0.13	0.13	0.13	0.13	0.13	0.13	0.13
$h$	0.72	0.72	0.72	0.72	0.72	0.72	0.72
$\frac{\chi''(1)}{\chi'(1)}$	5.09	5.09	5.11	5.13	5.09	5.09	5.09
$\kappa_p$	0.04	0.04	0.04	0.04	0.04	0.04	0.04
$\kappa_w$	0.01	0.01	0.01	0.01	0.01	0.01	0.01
$\nu$	3.71	3.71	3.68	3.65	<b>3.81</b>	<b>4.21</b>	<b>4.71</b>
$S''(1)$	6.93	6.95	7.02	7.11	6.92	6.89	6.86
$\rho_R$	0.58	0.58	0.58	0.58	0.58	0.58	0.59
$\phi_\pi$	1.54	1.539	1.537	1.534	1.541	1.546	1.550
$\phi_x$	0.006	0.006	0.006	0.006	0.006	0.006	0.007
$\rho$	0.85	0.85	0.85	0.85	0.85	0.85	0.85
$\rho_\mu$	0.31	0.31	0.31	0.30	0.31	0.31	0.31
$\rho_p$	0.88	0.88	0.88	0.88	0.88	0.88	0.88
$\phi_p$	0.58	0.58	0.58	0.58	0.58	0.58	0.57
$\rho_w$	0.99	0.99	0.99	0.99	0.99	0.99	0.99
$\phi_w$	0.54	0.54	0.53	0.53	0.54	0.56	0.57
$\rho_{mp}$	0.03	0.03	0.03	0.03	0.03	0.03	0.03
$\rho_g$	0.94	0.94	0.94	0.94	0.94	0.94	0.94
$\sigma_a$	1.43	1.43	1.43	1.44	1.43	1.43	1.44
$\sigma_s$	0.29	0.29	0.30	0.31	0.29	0.29	0.29
$\sigma_\mu$	18.63	<b>18.73</b>	<b>19.13</b>	<b>19.63</b>	18.63	18.63	18.63
$\sigma_p$	0.16	0.16	0.16	0.16	0.16	0.16	0.16
$\sigma_w$	0.44	0.44	0.44	0.44	0.44	0.43	0.42
$\sigma_{mp}$	0.38	0.38	0.38	0.38	0.38	0.38	0.38
$\sigma_g$	0.37	0.37	0.37	0.37	0.37	0.37	0.37

Note:  $\gamma_0^{med}$  corresponds to the posterior means under diagnostic expectations. The values are rounded to two decimal places except for  $\phi_x$ . Panel (a) shows results when all parameters can vary to minimize the KL criterion. Panel (b) shows results when  $\sigma_\mu$  is fixed at its baseline value. The bold value signifies the binding constraint.

Table 16: KL and empirical distances between  $\gamma_c$  and  $\gamma_0$ , HSY (2024) model

	(a) All parameters can vary			(b) $\sigma_\mu$ fixed		
	$c = 0.1$	$c = 0.5$	$c = 1.0$	$c = 0.1$	$c = 0.5$	$c = 1.0$
KL	6.49e-06	1.59e-04	6.24e-04	1.76e-05	3.81e-04	1.29e-03
T=80	0.0538	0.0714	0.0983	0.0556	0.0803	0.1150
T=150	0.0552	0.0797	0.1200	0.0578	0.0948	0.1510
T=200	0.0559	0.0848	0.1340	0.0591	0.1040	0.1750
T=1000	0.0634	0.1440	0.3090	0.0723	0.2190	0.4820

Note: KL denotes  $KL_{ff}(\gamma_0^{med}, \gamma_c^{med})$  with  $\gamma_0^{med}$  corresponding to the posterior means under diagnostic expectations. The empirical distance measure equals  $p_{ff}(\gamma_0^{med}, \gamma_c^{med}, 0.05, T)$ , where T is specified in the last four rows of the table. Panel (a) shows results when all parameters can vary. Panel (b) shows results when  $\sigma_\mu$  is fixed at its baseline value.  $\kappa_p = (\epsilon_p - 1)/\psi_p$ ,  $\kappa_w = (\omega\epsilon_w)/\psi_w$ . I follow [L’Huillier et al. \(2024\)](#) and calibrate  $\epsilon_p = \epsilon_w = 6$ ,  $\omega = 1$ .

## 4.2 Observable Equivalence and the Role of Frictions

In this subsection, I address the second research question: whether DE generates dynamics that are truly distinct from RE in a world with frictions, and how DE interacts with other frictions to produce these dynamics. Following the approach in Section 3.4, I fix the parameters of the benchmark DE model at their posterior means and search for parameter values of alternative models within feasible bounds that minimize the KL distance between the two spectra. The alternatives include the corresponding RE model as well as DE models with altered information frictions, reduced price or wage rigidity, and weaker habit formation. The results are summarized in Table 17.

First, I examine observable equivalence between the DE and RE specifications. The KL distance is 0.99 for  $T = 80$  and 1 for  $T = 150$ , indicating that no observable equivalence exists between DE and RE, even with a rich set of frictions. Among the parameters that shift most significantly, the medium-scale RE model requires weaker habit formation, more flexible prices and wages, more volatile markup shocks, and a more dovish monetary policy response to inflation in order to approximate the spectrum of the DE model. In addition, the inverse Frisch elasticity decreases substantially (from 3.71 to 2.39), implying a much more elastic labor supply under RE. These adjustments are intuitive. To replicate the stronger demand responses induced by DE consumers’ extrapolative expectations, RE consumers must rely less on past consumption habits. Since the RE Phillips curves lack extrapolative dy-

namics, prices must adjust more flexibly than under DE to reproduce observed behavior. Likewise, markup shocks become more volatile in the RE case because, without endogenous amplification from expectations, the model depends more heavily on exogenous shock variances. The sharp increase in labor supply elasticity reflects the RE model’s need for structural amplification to replicate the employment volatility that DE generates through behavioral amplification. Since RE agents do not overreact to shocks, workers must be far more responsive to wage changes to achieve comparable employment fluctuations. Finally, as argued by [L’Huillier et al. \(2024\)](#), when the intertemporal elasticity of substitution equals one, a hawkish monetary policy rule dampens the propagation of noise shocks in RE models. Hence, to mimic DE dynamics, the RE model requires an unrealistically dovish policy rule.

Interestingly, the noise shock variance to permanent productivity growth is lower in the RE case. Under RE with information frictions, agents tend to misperceive permanent productivity growth as transitory, which generates an underreaction mechanism. By contrast, DE amplifies noisy signals and creates an overreaction mechanism. To achieve near observable equivalence, the RE model which has no extrapolation therefore requires lower noise variance. This pattern contrasts with level shocks, where DE’s overreaction forces the RE model to compensate with higher shock variances. The reason for this contrast is that shocks to growth rates compound over time, making them much more persistent than level shocks and thus requiring a stronger underreaction mechanism to avoid excessive amplification. It is worth noting, however, that [L’Huillier et al. \(2024\)](#) analyze noise in productivity levels, so their results are not directly comparable to the growth rate specification considered here.

To further study the role of information frictions, I fix  $\sigma_s$  at alternative levels and allow the remaining parameters of the DE model to adjust in order to fit the benchmark DE spectrum. In particular, I compare a near-frictionless case ( $\sigma_s = 0.01$ ) with a high-friction case ( $\sigma_s = 1$ ). This exercise highlights how informational frictions reshape both the structural parameters and the degree of DE distortion required to replicate the benchmark dynamics. For the near-frictionless case, no observable equivalence is detected: the KL distance is 0.50 for  $T = 80$  and 0.719 for  $T = 150$ . The parameters remain close to those of the benchmark DE model. In particular, the DE distortion parameter decreases only slightly, from 0.73 to 0.70. The more notable changes occur in investment-related parameters. When DE agents can observe productivity growth almost perfectly, investment decisions respond less to spurious signals.

As a result, the model requires less volatility from marginal efficiency shocks. For the high-friction case, no observable equivalence is detected either: the KL distance equals 1 for both  $T = 80$  and  $T = 150$ . With severe information frictions, the underreaction channel becomes stronger, which in turn raises the required degree of diagnostic distortion. In this setting, the model relies more heavily on volatile investment specific shocks to generate sufficient fluctuations, while at the same time making capital utilization efficiency more costly to adjust. These adjustments reflect the economy’s need for stronger structural amplification when informational noise is large.

The next two columns in Table 17 examine the effects of relaxing price rigidity and wage rigidity. Again, no observable equivalence is detected. DE distortions are significantly reduced when either rigidity is relaxed, and the dynamics rely more heavily on exogenous shocks, with markup shocks becoming more volatile. In this sense, price rigidity acts as a competing channel to DE, but on its own it cannot generate dynamics as realistic as the benchmark DE specification. Notably, when wage rigidity is reduced, capital utilization becomes less costly. In both cases, investment adjustment costs are reduced and labor supply becomes more elastic, reflecting the model’s need to compensate for DE’s overreaction in investment and employment dynamics. Habit formation is also reduced, consistent with the diminished role of DE distortions in amplifying fluctuations.

Similarly, the habit formation column shows that lower habit formation can act as a competing channel for DE, particularly in consumption overreaction. No observable equivalence is detected as well. Reducing the degree of habit formation substantially decreases DE distortion, with  $\theta$  falling to 0.1 (the lower bound of the DE parameter). In this case, overreaction in investment and employment dynamics is absorbed more heavily through flexible labor supply and exogenous markup shocks.

In sum, these experiments show that DE generates dynamics distinct from RE. While other frictions can partially substitute for DE distortions by shifting extrapolation to other channels, none can fully replicate the benchmark DE dynamics. This suggests that DE captures a distinct endogenous amplification mechanism that cannot be mimicked by conventional frictions alone, underscoring its importance in explaining macroeconomic fluctuations.



Table 17: The closest models with DE vs RE, HSY (2024) model

	$\gamma_0^{med}$	$\theta = 0$	$\sigma_s = 0.01$	$\sigma_s = 1$	$\kappa_p = 0.1$	$\kappa_w = 0.1$	$h = 0.1$
KL	—	0.1160	0.0066	0.0481	0.0743	0.1060	0.6520
$T = 80$	—	0.9940	0.5000	1.0000	0.9600	0.9910	1.0000
$T = 150$	—	1.0000	0.7190	1.0000	0.9980	1.0000	1.0000
$\theta$	0.73	0.00	0.70	0.92	0.36	0.46	0.10
$\alpha$	0.13	0.14	0.14	0.11	0.13	0.14	0.13
$h$	0.72	0.56	0.72	0.73	0.66	0.67	0.10
$\frac{\chi''(1)}{\chi'(1)}$	5.09	4.94	4.48	6.60	4.99	3.96	4.98
$\kappa_p$	0.04	0.07	0.04	0.04	0.10	0.06	0.04
$\kappa_w$	0.01	0.04	0.01	0.01	0.02	0.10	0.05
$\nu$	3.71	2.39	3.56	3.13	3.08	2.30	2.30
$S''$	6.93	6.38	6.62	7.95	6.06	6.04	6.09
$\rho_R$	0.58	0.54	0.59	0.54	0.59	0.55	0.45
$\phi_\pi$	1.54	1.32	1.59	1.44	1.60	1.65	1.25
$\phi_x$	0.006	0.003	0.007	0.003	0.007	0.005	0.002
$\rho$	0.85	0.81	0.86	0.84	0.79	0.86	0.88
$\rho_\mu$	0.31	0.31	0.32	0.28	0.27	0.23	0.26
$\rho_p$	0.88	0.90	0.88	0.89	0.91	0.89	0.89
$\phi_p$	0.58	0.60	0.58	0.55	0.43	0.59	0.66
$\rho_w$	0.99	0.99	0.99	0.99	0.99	0.99	0.99
$\phi_w$	0.54	0.42	0.57	0.40	0.44	0.10	0.43
$\rho_{mp}$	0.03	0.03	0.01	0.07	0.01	0.01	0.01
$\rho_g$	0.94	0.94	0.94	0.93	0.94	0.94	0.92
$\sigma_a$	1.43	1.46	1.38	1.74	1.43	1.36	1.41
$\sigma_s$	0.29	0.18	0.01	1.00	0.24	0.19	0.10
$\sigma_\mu$	18.63	18.55	17.73	21.71	18.19	18.84	18.75
$\sigma_p$	0.16	0.22	0.16	0.14	0.21	0.20	0.20
$\sigma_w$	0.44	0.65	0.48	0.37	0.58	1.04	0.67
$\sigma_{mp}$	0.38	0.38	0.38	0.38	0.38	0.39	0.39
$\sigma_g$	0.37	0.37	0.37	0.37	0.37	0.37	0.37

Note: KL (the second row) and the empirical distance measure (the third and fourth row) are defined as  $KL_{ff}(\gamma_0^{med}, \gamma^{med})$  and  $p_{ff}(\gamma_0^{med}, \gamma^{med}, 0.05, T)$ . Each column contains a parameter vector that minimizes the KL criterion under a particular constraint on the friction. The optimizers are rounded to two decimal places except for  $\phi_x$ .

## 5 Conclusion

This paper provides the first comprehensive econometric analysis of DE in DSGE models. Methodologically, I extend SMC sampling to the indeterminacy domain and document systematic differences in identification outcomes relative to traditional MCMC methods. From

an economic perspective, I show that DE are identifiable both locally and globally. While incorporating DE does not compromise overall model identification, it consistently weakens the identification of shock variances, as the diagnostic parameter primarily distorts dynamics through shock propagation channels. More fundamentally, the paper demonstrates that DE generate macroeconomic dynamics distinct from those under RE, even for a medium-scale DSGE model with rich structural frictions. An observational equivalence analysis reveals that no parameterization of RE models can replicate the spectral properties of DE models. While other frictions can partially substitute for DE distortions by shifting extrapolation to alternative extrapolate channels, none can fully replicate the benchmark DE dynamics. This establishes DE as a unique and irreplaceable source of macroeconomic fluctuations. Ultimately, DE should be regarded not merely as an alternative modeling assumption, but as a distinct and economically meaningful departure from RE. The evidence presented here underscores that understanding macroeconomic fluctuations requires close attention to how agents form expectations, not only to frictions and exogenous shocks.

## References

- AN, S. AND F. SCHORFHEIDE (2007): “Bayesian analysis of DSGE models,” *Econometric reviews*, 26, 113–172.
- ANDERSON, G. S. (2008): “Solving linear rational expectations models: A horse race,” *Computational Economics*, 31, 95–113.
- BIANCHI, F., C. ILUT, AND H. SAIJO (2024a): “Diagnostic business cycles,” *Review of Economic Studies*, 91, 129–162.
- BIANCHI, F., C. L. ILUT, AND H. SAIJO (2024b): “Smooth diagnostic expectations,” Tech. rep., National Bureau of Economic Research.
- BLANCHARD, O. J., J.-P. L’HUILIER, AND G. LORENZONI (2013): “News, noise, and fluctuations: An empirical exploration,” *American Economic Review*, 103, 3045–3070.
- BORDALO, P., N. GENNAIOLI, S. Y. KWON, AND A. SHLEIFER (2021): “Diagnostic bubbles,” *Journal of Financial Economics*, 141, 1060–1077.
- BORDALO, P., N. GENNAIOLI, Y. MA, AND A. SHLEIFER (2020): “Overreaction in macroeconomic expectations,” *American Economic Review*, 110, 2748–82.
- BORDALO, P., N. GENNAIOLI, AND A. SHLEIFER (2018): “Diagnostic expectations and credit cycles,” *The Journal of Finance*, 73, 199–227.
- CAI, M., M. DEL NEGRO, E. HERBST, E. MATLIN, R. SARFATI, AND F. SCHORFHEIDE (2021): “Online estimation of DSGE models,” *The Econometrics Journal*, 24, C33–C58.
- CANOVA, F. AND L. SALA (2009): “Back to square one: Identification issues in DSGE models,” *Journal of Monetary Economics*, 56, 431–449.
- DEL NEGRO, M. AND F. SCHORFHEIDE (2008): “Forming priors for DSGE models (and how it affects the assessment of nominal rigidities),” *Journal of Monetary Economics*, 55, 1191–1208.
- GALÍ, J. (2015): *Monetary policy, inflation, and the business cycle: an introduction to the new Keynesian framework and its applications*, Princeton University Press.

- GUO, J., Y. LUO, AND P. YIN (2023): “Diagnostic Expectations and Consumption Dynamics,” *Available at SSRN 5173669*.
- HAZELL, J., J. HERRENO, E. NAKAMURA, AND J. STEINSSON (2022): “The slope of the Phillips Curve: evidence from US states,” *The Quarterly Journal of Economics*, 137, 1299–1344.
- HERBST, E. AND F. SCHORFHEIDE (2014): “Sequential Monte Carlo sampling for DSGE models,” *Journal of Applied Econometrics*, 29, 1073–1098.
- HERBST, E. P. AND F. SCHORFHEIDE (2016): *Bayesian estimation of DSGE models*, Princeton University Press.
- ISKREV, N. (2010): “Local identification in DSGE models,” *Journal of Monetary Economics*, 57, 189–202.
- JONES, C., M. KULISH, AND J. P. NICOLINI (2021): “Priors and the Slope of the Phillips Curve,” Tech. rep., JSTOR.
- KAHNEMAN, D. AND A. TVERSKY (1972): “Subjective probability: A judgment of representativeness,” *Cognitive psychology*, 3, 430–454.
- KOCIEŃKI, A. AND M. KOLASA (2023): “A solution to the global identification problem in DSGE models,” *Journal of Econometrics*, 236, 105477.
- KOMUNJER, I. AND S. NG (2011): “Dynamic identification of dynamic stochastic general equilibrium models,” *Econometrica*, 79, 1995–2032.
- KOOP, G., M. H. PESARAN, AND R. P. SMITH (2013): “On identification of Bayesian DSGE models,” *Journal of Business & Economic Statistics*, 31, 300–314.
- LUBIK, T. A. AND F. SCHORFHEIDE (2003): “Computing sunspot equilibria in linear rational expectations models,” *Journal of Economic dynamics and control*, 28, 273–285.
- (2004): “Testing for indeterminacy: An application to US monetary policy,” *American Economic Review*, 94, 190–217.

- L’HUIILLIER, J.-P., S. R. SINGH, AND D. YOO (2024): “Incorporating diagnostic expectations into the New Keynesian framework,” *Review of Economic Studies*, 91, 3013–3046.
- NA, S. AND D. YOO (2025): “Overreaction and macroeconomic fluctuation of the external balance,” *Journal of Monetary Economics*, 151, 103750.
- NAKAMURA, E. AND J. STEINSSON (2014): “Fiscal stimulus in a monetary union: Evidence from US regions,” *American Economic Review*, 104, 753–792.
- PLANAS, C., M. RATTO, AND A. ROSSI (2015): “Slice sampling in Bayesian estimation of DSGE models,” in *Conference paper presented at 11th DYNARE conference*.
- QU, Z. AND D. TKACHENKO (2012): “Identification and frequency domain quasi-maximum likelihood estimation of linearized dynamic stochastic general equilibrium models,” *Quantitative Economics*, 3, 95–132.
- (2017): “Global identification in DSGE models allowing for indeterminacy,” *The Review of Economic Studies*, 84, 1306–1345.
- (2023): “Using arbitrary precision arithmetic to sharpen identification analysis for DSGE models,” *Journal of Applied Econometrics*, 38, 644–667.
- SCHORFHEIDE, F. (2008): “DSGE model-based estimation of the New Keynesian Phillips curve,” *FEB Richmond Economic Quarterly*, 94, 397–433.
- SIMS, C. A. (2002): “Solving linear rational expectations models,” *Computational economics*, 20, 1.
- SMETS, F. AND R. WOUTERS (2007): “Shocks and frictions in US business cycles: A Bayesian DSGE approach,” *American economic review*, 97, 586–606.

## 6 Appendix

### 6.1 A small-scale DSGE model: Analytical solution

An intuitive way of understanding why adding diagnostic distortion weakens the identification strength of the shock variance relatively is to examine the analytical solution. Below, I present the analytical solution using the guess-and-verify method. To simplify the analysis, I consider a two-equation system, which is the benchmark system without the monetary policy rule and with the interest rate being constant:

$$\begin{aligned}
(1 + \theta)E_t[\hat{y}_{t+1}] + (1 + \theta)E_t[\hat{\pi}_{t+1}] - \hat{y}_t + \hat{g}_t + \theta\hat{\pi}_t - (1 + \theta)E_t[\hat{g}_{t+1}], \\
= \theta E_{t-1}[\hat{y}_{t+1}] + \theta E_{t-1}[\hat{\pi}_{t+1}] + \theta E_{t-1}[\hat{\pi}_t] - \theta E_{t-1}[\hat{g}_{t+1}], \\
\hat{\pi}_t = \beta(1 + \theta)E_t[\hat{\pi}_{t+1}] - \beta\theta E_{t-1}[\hat{\pi}_{t+1}] + \kappa(\hat{y}_t - \hat{a}_t) - \kappa\psi\hat{g}_t, \\
\hat{a}_t = \rho_a\hat{a}_{t-1} + \varepsilon_{a,t}, \quad \hat{g}_t = \rho_g\hat{g}_{t-1} + \varepsilon_{g,t}
\end{aligned}$$

Guess the solution is in the form of

$$\hat{y}_t = \alpha_{11}\hat{a}_{t-1} + \alpha_{12}\hat{g}_{t-1} + \mu_{11}\varepsilon_{a,t} + \mu_{12}\varepsilon_{g,t}, \quad \hat{\pi}_t = \alpha_{21}\hat{a}_{t-1} + \alpha_{22}\hat{g}_{t-1} + \mu_{21}\varepsilon_{a,t} + \mu_{22}\varepsilon_{g,t}$$

Plugging in the guess solution, collecting terms and comparing coefficient yields

$$\begin{aligned}
\alpha_{11} &= -\frac{\kappa\rho_a^2}{1 - \rho_a(1 + \beta + \kappa) + \beta\rho_a^2}, & \alpha_{12} &= \frac{\rho_g[1 - \rho_g(1 + \beta + \kappa\psi) + \beta\rho_g^2]}{1 - \rho_g(1 + \beta + \kappa) + \beta\rho_g^2} \\
\alpha_{21} &= -\frac{\kappa(1 - \rho_a)\rho_a}{1 - \rho_a(1 + \beta + \kappa) + \beta\rho_a^2}, & \alpha_{22} &= \frac{\kappa\rho_g(1 - \psi)(1 - \rho_g)}{1 - \rho_g(1 + \beta + \kappa) + \beta\rho_g^2} \\
\mu_{11} &= -\frac{\kappa[\rho_a + \theta(1 - \kappa\rho_a) + \beta\rho_a\theta^2(1 - \rho_a)]}{[1 - \rho_a(1 + \beta + \kappa) + \beta\rho_a^2](1 - \kappa\theta)}, & \mu_{12} &= (1 + \theta)(\alpha_{12} + \alpha_{22} - \rho_g) + \theta\mu_{22} + 1, \\
\mu_{21} &= -\frac{\kappa[(1 - \rho_a) + \rho_a\theta[\kappa + \beta(1 - \rho_a)]]}{[1 - \rho_a(1 + \beta + \kappa) + \beta\rho_a^2](1 - \kappa\theta)}, & \mu_{22} &= \frac{(1 + \theta)[\beta\alpha_{22} + \kappa(\alpha_{12} + \alpha_{22} - \rho_g)] + \kappa(1 - \psi)}{1 - \kappa\theta}.
\end{aligned}$$

where  $\alpha_{11}, \alpha_{12}, \alpha_{21}, \alpha_{22}$  are the same as in the RE case, while DE affects the shock terms  $\mu_{11}, \mu_{12}, \mu_{21}, \mu_{22}$ . This result is in line with the theoretical predictions. As demonstrated by [Bordalo et al. \(2018\)](#), DE induces overreaction in the dynamics of exogenous processes and, consequently, amplifies their effects on endogenous variables. Since the diagnosticity parameter  $\theta$  operates exclusively through the transmission of shocks to endogenous variables, the likelihood function becomes less sensitive to variations in shock variances. This diminished sensitivity implies that the data contain less information about these variances, thereby weakening their identification.

## 6.2 A medium scale DSGE

In this section I list the equations I used in section 4.1 which are same as the equations in the replication Dynare code of [L’Huillier et al. \(2024\)](#) except the information friction part.

### Non-stationary Productivity:

Productivity (in logs) is given by the sum of two components:

$$a_t = x_t + z_t.$$

The permanent component,  $x_t$ , follows a unit root process given by

$$\Delta x_t = \rho_x \Delta x_{t-1} + \varepsilon_{x,t}.$$

The transitory component,  $z_t$ , follows a stationary process given by

$$z_t = \rho_z z_{t-1} + \varepsilon_{z,t}.$$

[Blanchard et al. \(2013\)](#) assume  $a_t$  is a unit root process

$$a_t = a_{t-1} + \varepsilon_{a,t}, \tag{23}$$

with the variance of  $\varepsilon_{a,t}$  equal to  $\sigma_a^2$ . In general, a given univariate process is consistent with an infinity of decompositions between a permanent and a transitory component with orthogonal innovations. [Blanchard et al. \(2013\)](#) choose one-parameter family which deliver

the above univariate random walk:

$$\rho_x = \rho_z = \rho, \quad \sigma_x^2 = (1 - \rho)^2 \sigma_a^2, \quad \sigma_z^2 = \rho \sigma_a^2,$$

Consumers observe current and past productivity,  $a_t$ . In addition, I assume they receive a signal about permanent productivity growth.<sup>14</sup>

$$s_t = \Delta x_t + \varepsilon_{s,t},$$

where  $\varepsilon_{s,t}$  is i.i.d. normal with variance  $\sigma_s^2$ . Moreover, consumers know the structure of the model, i.e., know  $\rho$  and the variances of the three shocks.

#### Kalman Filter:

Following [L’Huillier et al. \(2024\)](#), I employ the Kalman filter as a computational tool to transform an incomplete information model into a form that mimics complete information while preserving the economic intuition of agents learning from signals. Since the global identification condition requires the spectral density to be nonsingular, I follow [Qu and Tkachenko \(2023\)](#) and define the unit root variable in growth rates. The state equations are:

$$\Delta x_t = \rho_x \Delta x_{t-1} + \varepsilon_{x,t}$$

$$z_t = \rho_z z_{t-1} + \varepsilon_{z,t}$$

$$z_{t-1} = z_{t-1}.$$

The observation equations are:

$$\Delta a_t = \Delta x_t + z_t - z_{t-1}$$

$$s_t = \Delta x_t + \varepsilon_{s,t}.$$

---

<sup>14</sup>[L’Huillier et al. \(2024\)](#) assume that consumers observe a signal on the level of the permanent productivity component. I modify this assumption to stabilize the general equilibrium system; otherwise, the optimization converges very slowly due to the presence of a unit root.



I write the above system in matrix form as:

$$\mathbf{X}_t = \mathbf{F}\mathbf{X}_{t-1} + \boldsymbol{\varepsilon}_t \quad (24)$$

where

$$\mathbf{X}_t = \begin{bmatrix} \Delta x_t \\ z_t \\ z_{t-1} \end{bmatrix}, \quad \mathbf{F} = \begin{bmatrix} \rho_x & 0 & 0 \\ 0 & \rho_z & 0 \\ 0 & 1 & 0 \end{bmatrix}, \quad \boldsymbol{\varepsilon}_t = \begin{bmatrix} \varepsilon_{x,t} \\ \varepsilon_{z,t} \\ 0 \end{bmatrix},$$

and

$$\mathbf{Y}_t = \mathbf{A}\mathbf{X}_t + \boldsymbol{\eta}_t \quad (25)$$

where

$$\mathbf{Y}_t = \begin{bmatrix} \Delta a_t \\ s_t \end{bmatrix}, \quad \mathbf{A} = \begin{bmatrix} 1 & 1 & -1 \\ 1 & 0 & 0 \end{bmatrix}, \quad \boldsymbol{\eta}_t = \begin{bmatrix} 0 \\ \varepsilon_{s,t} \end{bmatrix}.$$

Following [L'Huillier et al. \(2024\)](#), I employ the Kalman filter as a computational tool to transform an incomplete information model into a form that mimics complete information:

$$\begin{aligned} \begin{pmatrix} \Delta x_{t|t} \\ z_{t|t} \\ z_{t-1|t} \end{pmatrix} &= (\mathbf{I} - \mathbf{K}\mathbf{A})\mathbf{F} \begin{pmatrix} \Delta x_{t-1|t-1} \\ z_{t-1|t-1} \\ z_{t-2|t-1} \end{pmatrix} + \mathbf{K} \begin{pmatrix} \Delta a_t \\ s_t \end{pmatrix} \\ &= \mathbf{F} \begin{pmatrix} \Delta x_{t-1|t-1} \\ z_{t-1|t-1} \\ z_{t-2|t-1} \end{pmatrix} + \underbrace{\mathbf{K} \left[ \begin{pmatrix} \Delta a_t \\ s_t \end{pmatrix} - \mathbf{A}\mathbf{F} \begin{pmatrix} \Delta x_{t-1|t-1} \\ z_{t-1|t-1} \\ z_{t-2|t-1} \end{pmatrix} \right]}_{\equiv \mathbf{e}_t}, \end{aligned} \quad (26)$$

$$\Rightarrow \begin{pmatrix} \Delta a_t \\ s_t \end{pmatrix} = \mathbf{A}\mathbf{F} \begin{pmatrix} \Delta x_{t-1|t-1} \\ z_{t-1|t-1} \\ z_{t-2|t-1} \end{pmatrix} + \mathbf{e}_t, \quad (27)$$

where  $\mathbf{K}$  the steady-state, time-invariant Kalman gain obtained from the Riccati recursion. Equation (26) and (27) are incorporated into the general equilibrium system.

$$\begin{aligned}
\hat{\lambda}_t - \hat{G}_{a,t} - \hat{\pi}_t &= \hat{i}_t + \mathbb{E}_t^\theta[\hat{\lambda}_{t+1} - \hat{G}_{a,t} - \hat{G}_{a,t+1} - \hat{\pi}_t - \hat{\pi}_{t+1}] \\
\hat{\lambda}_t + \frac{G_a}{G_a - h} \hat{c}_t - \frac{h}{G_a - h} (\hat{c}_{t-1} - \hat{G}_{a,t}) &= 0 \\
\hat{\pi}_t &= \beta \mathbb{E}_t^\theta[\hat{\pi}_{t+1} - \iota_p \hat{\pi}_t] + \iota_p \hat{\pi}_{t-1} + \frac{\epsilon_p - 1}{\psi_p} \hat{m}c_t + \hat{\lambda}_t^{p,*} \\
\hat{\pi}_t^w &= \beta \mathbb{E}_t^\theta[\hat{\pi}_{t+1}^w - \iota_w \hat{\pi}_t - \iota_w \hat{G}_{a,t+1}] + \iota_w \hat{\pi}_{t-1} + \iota_w \hat{G}_{a,t} + \frac{\epsilon_w \omega L^{1+\nu}}{\psi_w} [\nu \hat{L}_t - \hat{w}_t - \hat{\lambda}_t] + \hat{\lambda}_t^{w,*} \\
\hat{k}_{t+1}^u &= \frac{\mathbb{I}}{k^u} (\hat{I}_t + \hat{\mu}_t) + \frac{1 - \delta_k}{G_a} (\hat{k}_t^u - \hat{G}_{a,t}) \\
\hat{q}_t - \hat{G}_{a,t} + \hat{\lambda}_t &= \mathbb{E}_t^\theta[\hat{\lambda}_{t+1} - \hat{G}_{a,t} - \hat{G}_{a,t+1} + \frac{r^K}{r^K + 1 - \delta_k} \hat{r}_{t+1}^K + \frac{1 - \delta_k}{r^K + 1 - \delta_k} \hat{q}_{t+1}] \\
\hat{q}_t + \hat{\mu}_t - S''(1)(\hat{I}_t - \hat{I}_{t-1} + \hat{G}_{a,t}) + \beta S''(1) \mathbb{E}_t^\theta[\hat{I}_{t+1} - \hat{I}_t + \hat{G}_{a,t+1}] &= 0 \\
\hat{k}_t &= \hat{u}_t + \hat{k}_t^u - \hat{G}_{a,t} \\
\hat{r}_t^K &= \frac{\chi''(1)}{\chi'(1)} \hat{u}_t \\
\hat{y}_t &= \alpha \hat{k}_t + (1 - \alpha) \hat{L}_t \\
\hat{r}_t^K &= \hat{w}_t + \hat{L}_t - \hat{k}_t \\
\hat{m}c_t &= \alpha \hat{r}_t^K + (1 - \alpha) \hat{w}_t \\
\hat{i}_t &= \rho_R \hat{i}_{t-1} + (1 - \rho_R)(\phi_\pi \hat{\pi}_t + \phi_y \hat{y}_t) + \hat{\lambda}_t^{mp} \\
\frac{1}{\lambda^g} \hat{y}_t &= \frac{c}{y} \hat{c}_t + \frac{\mathbb{I}}{y} \hat{I}_t + \frac{\chi'(1)k}{y} \hat{u}_t + \frac{1}{\lambda^g} \hat{\lambda}_t^g \\
\hat{\mu}_t &= \rho_\mu \hat{\mu}_{t-1} + \varepsilon_{\mu,t} \\
\hat{\lambda}_t^{mp} &= \rho_{mp} \hat{\lambda}_{t-1}^{mp} + \varepsilon_{mp,t} \\
\hat{\lambda}_t^g &= \rho_g \hat{\lambda}_{t-1}^g + \varepsilon_{g,t} \\
\hat{\lambda}_t^{p,*} &= \rho_p \hat{\lambda}_{t-1}^{p,*} + \varepsilon_{p,t} - \phi_p \varepsilon_{p,t-1} \\
\hat{\lambda}_t^{w,*} &= \rho_w \hat{\lambda}_{t-1}^{w,*} + \varepsilon_{w,t} - \phi_w \varepsilon_{w,t-1}
\end{aligned}$$

**Disturbances:**

TFP growth shock:	$\varepsilon_{x,t} \sim N(0, \sigma_x^2)$
Stationary TFP shock:	$\varepsilon_{z,t} \sim N(0, \sigma_z^2)$
Noise shock:	$\varepsilon_{s,t} \sim N(0, \sigma_s^2)$
MEI shock:	$\varepsilon_{\mu,t} \sim N(0, \sigma_\mu^2)$
Monetary policy shock:	$\varepsilon_{mp,t} \sim N(0, \sigma_{mp}^2)$
Government spending shock:	$\varepsilon_{g,t} \sim N(0, \sigma_g^2)$
Price markup shock:	$\varepsilon_{p,t} \sim N(0, \sigma_p^2)$
Wage markup shock:	$\varepsilon_{w,t} \sim N(0, \sigma_w^2)$